Environmental Microbiology

ENVIRONMENTAL MICROBIOLOGY

RESEARCH ARTICLE

Microbial Community of a Sandy Beach Subterranean Estuary is Spatially Heterogeneous and Impacted by Winter Waves

Jessica A. Bullington[1] | Kathryn Langenfeld[2] | Jacob R. Phaneuf[2] | Alexandria B. Boehm[2,3] | Christopher A. Francis[1,3]

[1]Department of Earth System Science, Stanford University, Stanford, California, USA | [2]Department of Civil and Environmental Engineering, Stanford University, Stanford, California, USA | [3]Department of Oceans, Stanford University, Stanford, California, USA

Correspondence: Alexandria B. Boehm (aboehm@stanford.edu) | Christopher A. Francis (caf@stanford.edu)

Received: 24 July 2024 | **Revised:** 22 October 2024 | **Accepted:** 15 November 2024

Funding: This work was supported by the U.S. National Science Foundation 'Understanding the Rules of Life: Microbiome Theory and Mechanisms' (URoL: MTM) Award # 2024504, Stanford University McGee and Levorsen Research Grant, and ARCO Stanford University Graduate Fellowship.

Keywords: coastal aquifer | fluorescent dissolved organic matter | microbial ecology | permeable sediment | submarine groundwater discharge | subterranean estuary

ABSTRACT

Subterranean estuaries (STEs) are critical ecosystems at the interface of meteoric groundwater and subsurface seawater that are threatened by sea level rise. To characterize the influence of tides and waves on the STE microbial community, we collected porewater samples from a high-energy beach STE at Stinson Beach, California, USA, over the two-week neap-spring tidal transition during both a wet and dry season. The microbial community, analyzed by 16S rRNA gene (V4) amplicon sequencing, clustered according to consistent physicochemical features found within STEs. The porewater community harbored relatively abundant Proteobacteria, Verrucomicrobiota, and Bacteroidota, as well as members of the archaeal DPANN superphylum and bacterial Candidate Phyla Radiation (CPR). Tidal conditions were not associated with microbial community composition; however, a wave overtopping event significantly impacted the beach microbiome. As a baseline for environmental change, our results elucidate the unique dynamics of a STE microbiome with unprecedented temporal resolution, highlighting the transport of cellular material through beach porewater due to waves.

1 | Introduction

Sandy beaches cover 31% of the Earth's unfrozen shoreline (Luijendijk et al. 2018) at the interface of land and sea. Beneath the sand surface, subterranean estuaries (STEs) within coastal aquifers are critical mixing zones of meteoric groundwater and subsurface seawater (Moore 1999; Rocha et al. 2021). STEs regulate the rate and chemical constituents of submarine groundwater discharge (SGD) to the ocean (Robinson et al. 2018), thereby mitigating eutrophication, harmful algal blooms, and deoxygenation in coastal waters (Lecher and Mackey 2018; Lee et al. 2010; Liefer et al. 2009; Moore et al. 2024). STEs have been termed natural "biogeochemical reactors" (Anschutz et al. 2009) due to their steep chemical gradients and microbially-mediated transformations. Despite their importance, the physical, chemical, and biological drivers of these processes remain unclear for STE environments. Elucidating the microbial contribution to biogeochemical cycling and physiological response to environmental changes will be critical to understanding STE ecosystem services,

Jessica A. Bullington and Kathryn Langenfeld are co-first authors.

particularly as rising sea levels modify and erode beach habitats (Brown and McLachlan 2002; Cooper et al. 2020; Defeo et al. 2009; Vousdoukas et al. 2020).

In the past decade, there has been increasing interest in characterizing the microbial community within STEs (Archana, Francis, and Boehm 2021; Ruiz-González, Rodellas, and Garcia-Orellana 2021). The steep physicochemical gradients of STEs, within tens of meters, are ideal for studying the environmental controls of microbial populations without the confounds of geographic variation present in most surface estuaries. Early works targeted mapping the distribution of microbes capable of nitrification and denitrification (Rogers and Casciotti 2010; Sáenz et al. 2012; Santoro, Boehm, and Francis 2006; Santoro et al. 2008). Whole community analyses (Adyasari et al. 2019; Chen et al. 2019; Hong et al. 2019; McAllister et al. 2015; Ye et al. 2016) discovered distinct microbial communities from fresh and marine groundwater that are impacted by the bidirectional flow and level of connectivity to seawater. The primary environmental factors that appear to correlate with variations in microbial community composition include salinity, dissolved oxygen (DO), temperature, dissolved inorganic nitrogen (DIN), and dissolved organic carbon (DOC).

However, there remain several important knowledge gaps in understanding what factors structure these communities. Despite significant variations in hydrology and chemistry of STEs due to tides (Robinson, Li, and Barry 2007; Robinson et al. 2018; Heiss and Michael 2014), the microbial community dynamics over fortnightly spring-neap, or daily and sub-daily tidal fluctuations, have not been investigated. Incorporating tidal variation into microbial profiling may be necessary to accurately capture baseline microbial dynamics in order to isolate the effects of sea level rise on STEs. Additionally, metrics of dissolved organic matter (DOM) quality, such as fluorescence (fDOM), have been used to distinguish sources of SGD in nearshore environments (Nelson et al. 2015). Application of these techniques to characterize DOM across the steep geochemical gradients of a STE may provide additional context for microbial distributions. Furthermore, only a few studies (Calvo-Martin et al. 2022; Degenhardt et al. 2020, 2021) have evaluated microbial diversity of STEs at sandy beaches where the coast is exposed to high-energy waves.

To address these critical knowledge gaps, we used 16S rRNA amplicon sequencing analysis paired with hydrological and physicochemical measurements to characterize a high-energy beach STE in Northern California (Stinson Beach, CA, USA). We collected samples at fine spatial scale (meter to sub-meter) and temporal resolution (sub-daily during high and low tides) over the spring-neap tide transition during February (rainy season) and October (dry season) of 2022. Previous physicochemical characterization of this beach identified freshening and nutrification of the coastal ocean during neap tides due to the discharge of nutrient-enriched groundwater from the STE (de Sieyes et al. 2008). Stinson Beach also experiences approximately six times greater groundwater discharge rates during the rainy season compared to the dry season (de Sieyes et al. 2011). While no previous microbial assessments have been conducted here, similar studies of high-energy sites report diverse yet seasonally consistent core communities (Calvo-Martin et al. 2022; Degenhardt et al. 2020, 2021). Our primary objectives were to evaluate the spatiotemporal and physicochemical controls of the microbial community structure and composition, as well as the disturbance of a set of winter waves (i.e. an overtopping event) on the community composition of the Stinson Beach STE.

2 | Materials and Methods

2.1 | Study Site

Sample collection was conducted at Stinson Beach, CA, USA (N 37.89901°, W 122.64521°) at four sites ("wells") from the STE along a cross-shore transect beginning at Well 1 and extending to the high tide line (Figure 1). The beach was surveyed using a scope and stick with reference to mean sea level (MSL) on 26 February 2022 and 12 October 2022 at low-low tide. Along the sampling transect, the top of the water table was approximately 1.5 m beneath the sand surface. Beach sediments were comprised of a mixture of very fine sand (6.25–125 μm diameter) to very coarse sand (1–2 mm) with heterogeneous ribbons of granules (2–4 mm) and pebbles (4–65 mm) and a clay aquitard (1–2 m beneath MSL).

The beach is an open-ocean, southwest-facing beach with mixed semidiurnal tides and a mean tide range of 0.89 m. The climate is Mediterranean with rainfall occurring predominantly between October and April. Two sampling campaigns were conducted from 23 February to 3 March 2022 (henceforth "February" sampling) and 11–18 October 2022 ("October" sampling). During February sampling, there was a rain event on March 3 from 7:00 to 19:00 PST peaking at 10:00 with a total accumulation of 8.89 mm. At the time of the October sampling, no rainfall had occurred during the preceding 2 months, and no rainfall occurred during sampling. The average air temperature during February and October sampling was 9.42 and 12.82°C, respectively. Households are located on the beach within 60 m of the surf with on-site septic systems and holding tanks for wastewater disposal.

2.2 | Sample Collection

Water samples were collected at every well and depth (Figure 1) twice daily at high-high (H) and low-low (L) tides to capture a spring-neap transition in February and October of 2022. Additional samples were collected at ebb tide defined as 1 h after H (referred to as M hereafter) in October. All together, a total of 516 STE porewater and 25 seawater surf samples were collected over 9 days in February and 8 days in October. Measurements for temperature, salinity, DO, pH, DIN, and dissolved inorganic phosphate were performed for all samples. For a select 182 porewater and 5 seawater surf samples, measurements for DOC, fDOM, microbial cell counts and microbial DNA extractions for 16S rRNA gene analysis were performed for 10 time points in February and 3 in October. Replicate samples, defined as samples collected at the exact same location and time, were not collected. One field blank was collected for each of the 13 timepoints where all measurements were performed using MilliQ water instead of sample water.

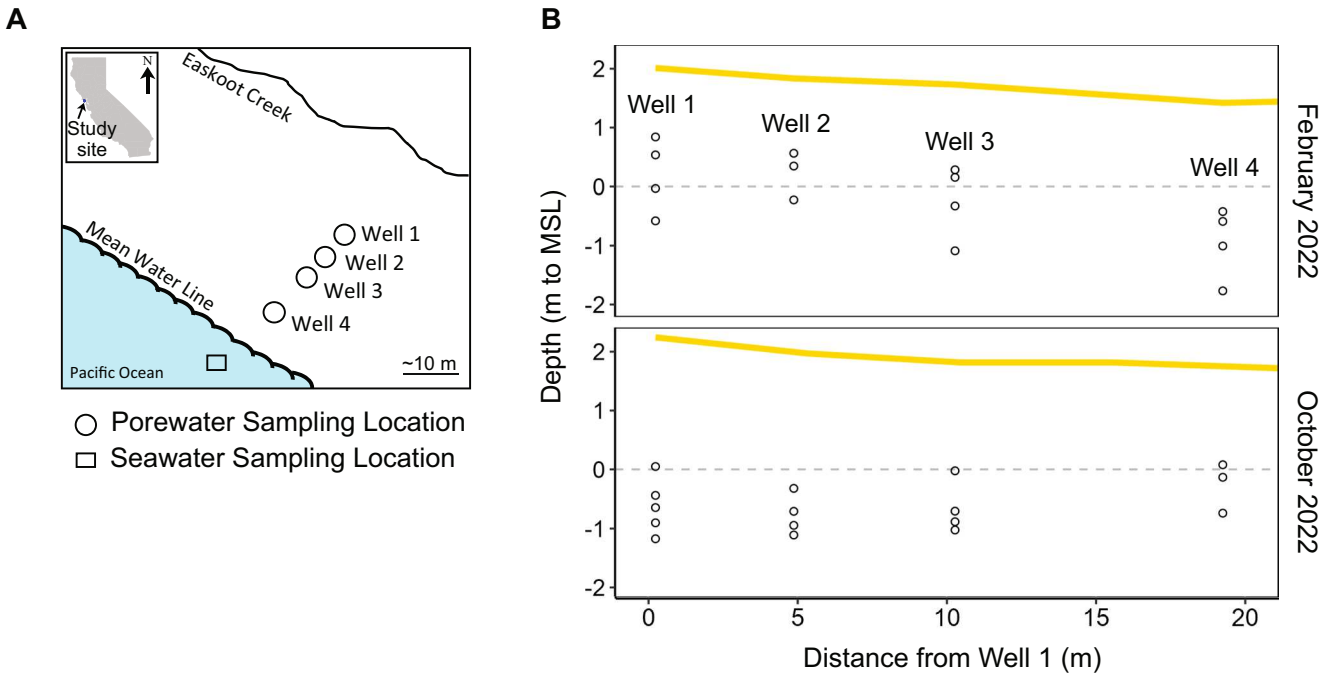

FIGURE 1 | Cross-shore transect at Stinson Beach, CA, USA, used to sample the subterranean estuary. Physicochemical ($n = 516$) and microbiological ($n = 182$) porewater samples were collected from four well locations (A) at several depths beneath the water table surface (B). Additional seawater surf samples for physicochemical ($n = 25$) and microbiological ($n = 5$) analyses were collected as a coastal reference. Sampling was conducted sub-daily at high-high (H) and low-low (L) tides during a spring-neap tidal transition in February (wet season) and October (dry season) of 2022 spanning 8–9 days each season. Additional ebb tide (M) samples were collected during October sampling. The yellow line indicates the surveyed sand surface. MSL refers to mean sea level. Eskoot Creek is a seasonal creek ~90 m landward of the MSL water line.

During the sampling events, slotted PVC wells were installed within 2 m of Well 1 (N 37.89901°, W 122.64521°) and Well 4 (N 37.89888°, W 122.64536°) with pressure transducers (Solinst, Levelogger Gold Model 3001) to measure water height every 5 min during February sampling and every minute during October sampling. At each well location, a sampling port was installed in the sand at several depths beneath the water table in February and October (Figure 1B). Ports consisted of polyethylene tubing with a two-inch screen and stainless-steel tip (M.H.E. Products, SedPoint2; Figure A1). Porewater was simultaneously pumped from each depth (~100 mL per minute) with a multi-head peristaltic pump at each well location and immediately filtered through 80-μm pore size autoclaved nylon mesh (McMaster-Carr, Cat. No. 9318T22) pre-rinsed with sample water. The mesh filtrate was collected in polyethylene containers that were washed with 10% hydrochloric acid, deionised water, and then triple rinsed with sample water.

Sensors and probes were used in the field to measure temperature and salinity (YSI, Model 30-10FT), DO (YSI, Cat. No. 14-660-204), and pH (Hanna Instruments, Cat. No. HI98107). Additional aliquots of the ~2.5 L of mesh filtrate, which was stored on ice in a cooler, were processed in an onsite lab within 3 h of collection for additional measurements, as described below.

2.3 | Inorganic Nutrient Measurements

Water samples for DIN and phosphate measurements were filtered using 0.22-μm pore size syringe filters (Millipore, Cat. No. 13-100-106) and stored in sterile polyethylene containers. Samples were then transported on dry ice in a cooler and stored at −20°C until processing (within 2 months). Ammonium was measured using the colorimetric salicylate-hypochlorite method (Bower and Holm-Hansen 1980). Nitrite and nitrate were measured using the Griess colorimetric assay on a SmartChem200 Discrete Analyser (Wada and Hattori 1971; Wood, Armstrong, and Richards 1967). Orthophosphate was measured using the molybdenum blue colorimetric assay (Murphy and Riley 1962; Nagul et al. 2015).

2.4 | Organic Matter Measurements

Water samples for DOC and fDOM were filtered using GF/F filters (Whatman, Cat No. 09-874-64) and stored in borosilicate vials (Fisher Scientific, Cat No. 02-912-380) that had been combusted at 450°C for 4 h prior to sample collection. Samples were then transported on dry ice in a cooler and stored at −20°C until processing (approximately 10 months). DOC and total dissolved nitrogen (TDN) were measured using a Shimadzu High-Temperature TOC-L Combustion Analyser after acidification to pH 2 with hydrochloric acid (Suzuki, Sugimura, and Itoh 1985; Suzuki, Tanoue, and Ito 1992). Samples for fDOM were analyzed using a Horiba Aqualog scanning fluorometer (Nelson et al. 2015). Biogeochemically relevant metrics and indices were calculated using the fluorescence intensity of known spectral peaks in excitation-emission matrices. We used 11 total fDOM metrics and indices. Further information is located in "Detailed Fluorescent Dissolved Organic Matter Methods" section in Appendix A.

2.5 | Cell Counts

Samples for cell counts were fixed with 32% paraformaldehyde (Fisher Scientific, Cat. No. AA47377-9 M) at a final concentration of 2% for 20 min at room temperature and then flash-frozen in liquid nitrogen. Samples were then transported on dry ice in a cooler and stored at −80°C until processing (approximately 8 months). DAPI-stained cells filtered onto 0.1-μm pore size Isopore membrane filters (Millipore, Cat. No. VCTP02500) were imaged and counted using a Nikon Eclipse Ti inverted epifluorescence microscope at 100× resolution. Further details are outlined in "Detailed Cell Count Methods" section in Appendix A.

2.6 | DNA Extraction

Samples for microbial DNA extractions were filtered onto 0.22-μm pore size PES filters (Millipore, Sterivex Cat. No. SVGP01050) until the filter clogged or ~1.5 L of sample water had passed through the filter (volumes ranged from 0.12 to 1.84 L, median of 1.52 L). The filters were then flash-frozen in liquid nitrogen, transported on dry ice in a cooler, and stored at −80°C until DNA was extracted (within 2 months). DNA extractions were performed using the AllPrep PowerViral DNA/RNA Kit (QIAGEN, Cat. No. 28000-50) and QIAcube Connect (QIAGEN, Cat. No. 9002864) with manufacturer modifications for prokaryotic cell DNA extraction including bead beating and chemical lysis. Five sterile filters were run in parallel during the sample DNA extractions as negative controls (hereafter, referred to as a 'kitome'). Further details on DNA extractions are provided in "Detailed DNA Extraction Methods" section in Appendix A.

2.7 | 16S rRNA Gene Amplicon Sequencing and Analysis

V4 16S rRNA gene amplicon sequencing with an Illumina MiSeq v2 was performed by the University of Michigan Microbiome Core using the modified 515 forward (5′-GTGYCAGCMGCCGCGGTAA-3′) and 806 reverse (5′-GGACTACNVGGGTWTCTAAT-3′) primers (Walters et al. 2015). A total of 200 samples were sequenced including 134 porewater samples from February, 48 porewater samples from October, five seawater surf samples, five field blanks, six kitome blanks, and two PCR negatives. Replicates of the same location and time were not included. Briefly, sequences were processed with the DADA2 pipeline (v1.22.0, Callahan et al. 2016), and resulting amplicon sequence variants (ASVs) were assigned taxonomic information with the SILVA nr99 database (v138.1, Quast et al. 2013; Yilmaz et al. 2014). ASVs with greater frequency and prevalence in the kitome and PCR-negative controls were deemed contaminants and removed with Decontam (v1.14.0, Davis et al. 2018). There were 7,613,584 total reads in the resulting dataset with 63,344 total unique ASVs. The median sequencing depth was 33,353 reads with a range from 7816 to 92,556 reads per sample. Detailed information on sequence processing can be found in "Detailed 16S rRNA Gene Sequencing Methods" section in Appendix A.

2.8 | Statistical Analyses

We tested the null hypothesis that there was no effect of location, season, or tide on physicochemical measurements and microbial communities. All statistical analyses were performed in R (v4.3.0, R Core Team 2023). To test the hypotheses for the environmental physicochemical data, we used the Kruskal-Wallis test (*kruskal.test* function in the base R stats package, R Core Team 2023). This non-parametric test was appropriate as untransformed and log-transformed data were non-normally distributed as determined using the Shapiro-Wilk test (*shapiro.test*). All p values were adjusted with the Bonferroni method with significance defined by an alpha of 0.05. Pairwise Spearman's rank correlations between physicochemical variables were computed with the *cor* function in the stats package and visualised with the *pheatmap* function and package (Kolde 2019). Variables with a correlation coefficient over 0.8 were considered collinear, and only one of the collinear variables was chosen for downstream analysis to reduce model inflation (Figure A2).

A total of 187 samples were analyzed using V4 16S rRNA gene sequencing including porewater and seawater samples from February and October. Sequencing read counts were transformed using the arcsin hyperbolic transform (Huber et al. 2002). Trends in results were the same with and without rarefaction (random subsampling to the same reads per sample, data not shown). Non-rarified analyses are reported herein (McMurdie and Holmes 2014). Samples with incomplete environmental data ($n = 4$ out of 187) were excluded from analyses for consistency between statistical tests. Based on the Bray-Curtis distance matrix, samples were clustered with the *hclust* function and visualised with the *heatmap* function using the stats package (Figure A3).

Spatiotemporal variation in microbial data was analyzed using constrained analysis of principal coordinates (CAP) of the Bray-Curtis distance matrix computed using the *ordinate* function in phyloseq (McMurdie and Holmes 2013) and *capscale* function in vegan (Dixon 2003; Oksanen et al. 2022). Physicochemical variables correlated with CAP axes were extracted with the *scores* function in vegan. Scores were considered significant if above sqrt (1/n), where n was the number of variables included in the analysis.

Physicochemical variables correlated with the microbial community were additionally analysed using *bioenv* (Clarke and Ainsworth 1993) in vegan. After removal of environmental co-variates (Figure A2), 2,047 statistical models were compared using all combinations of 11 variables: salinity, temperature, DO, pH, nitrate, nitrite, ammonia, phosphate, DOC, HIX (a fDOM metric related to humic content and extent of organic matter degradation), and Fpeak (a fDOM metric related to phenylalanine-like, proteinaceous DOM). The best model uses a set of independent variables that maximizes the rank correlation of the scaled Euclidean distances to the Bray–Curtis dissimilarity matrix of microbial community ASVs based on Mantel tests.

To test the effect of season, tidal regime (spring/neap), and tide (H/L), porewater microbial communitites were evaluated for

homogeneity of group dispersion (PERMDISP) using *betadisper*, analysis of similarity (ANOSIM) using *anosim*, and permutational multivariate analysis of variance (PERMANOVA) using *adonis2* in the vegan package. ANOSIM and PERMANOVA were used in tandem as complementary non-parametric rank-based and semi-parametric distance-based approaches (Somerfield, Clarke, and Gorley 2021).

Taxonomic shifts between samples were analyzed by mapping distributions across the transect through time. Visual representations were generated with phyloseq and ggplot2 (Wickham 2016), where taxa were aggregated at the phylum or genus level. For the reported relative abundances, the percent of total sequence reads rather than an average across samples was used. Indicator ASVs of region clusters and seawater infiltration were determined using the *DESeq* function in DESeq2 (Love, Huber, and Anders 2014), which uses the negative binomial generalised linear model and Wald statistic.

3 | Results

Physicochemical ($n = 516$) and microbiological ($n = 182$) porewater samples were collected from four well locations at several depths beneath the water table surface along a cross-shore transect of a high-energy beach in Northern California (Figure 1). Additional seawater surf samples for physicochemical ($n = 25$) and microbiological ($n = 5$) analyses were collected as coastal end members to contextualize the STE system. Sampling was conducted sub-daily at high-high (H) and low-low (L) tides during a spring-neap tidal transition in February (wet season) and October (dry season) of 2022 spanning 8–9 days each season. Additional ebb tide (M) samples were collected during October sampling.

3.1 | Environmental Variability

The Stinson Beach STE is hydrologically dynamic. In February, there was a net recharge of the beach aquifer during the neap-to-spring tide transition and a net discharge in October (Figure 2A). Net recharge was interpreted as an increase in the baseline water level for both Wells 1 and 4. Net discharge is a decline in the baseline water level. For both February and October of 2022, tidal amplitudes were reduced at Well 1 compared to Well 4. The difference in water level between Well 1 and Well 4 was used to calculate the water height gradient and the resulting direction of water flow (Figure 2B). Flow direction was generally oceanward with landward flow primarily restricted to high tides in both seasons. Overall, water movement was variable and dynamic over short time scales (~ hours).

For all physicochemical variables measured, there was a significant difference in values between wells and between depths (p values < 0.001; Table A1). A prominent feature consistent across seasons and tides was the significant difference between Well 4 and Wells 1–3. Well 4 samples had higher salinity, lower inorganic nutrient concentrations, and lower DOC and fDOM values (Table 1; Tables A2 and A3), confirming enhanced exchange with seawater. Within Wells 1–3, there were three distinct depth regions consistent across seasons and tides, including a shallow, intermediate, and deep layer. Notably, the salinity and DIN concentrations were unique between the layers. The shallow layer (0.0 to 1.0 m above MSL) had low salinity, the highest concentrations of nitrate, pockets of high nitrite (maximum 112.2 μM), and low ammonia (Table 1, Figure 3). The intermediate layer (−0.5 to 0.0 m below MSL) had low salinity, intermediate nitrate, intermediate nitrite, and low ammonia. The deep layer (−1.0 to −0.5 m below MSL) had higher salinity, lower nitrate, lower nitrite, and the highest ammonia (maximum 53.0 μM).

There were significant differences between porewater samples collected in February and October (p values < 0.001) for temperature, pH, nitrate, nitrite, and ammonia. Nitrate and pH were higher for samples collected in February, whereas temperature, nitrite, and ammonia were higher in October. There were no significant differences between measurements made at H and L tides (p value > 0.05), even within each region, season, or tidal regime (spring/neap).

The transition from neap to spring tide in February coincided with a wave set overtopping at Well 4 during the H tide on the 27th of February. Seawater subsequently infiltrated and mixed into the STE porewater impacting all wells (Figure 4). Pre- and post-overtopping, there were significant differences (p value < 0.001) in salinity, nitrate, phosphate, and fDOM values. Salinity increased post-overtopping while inorganic nutrients and fDOM metrics decreased. Notably, there were no significant differences in the deep February samples when analyzed independently. No overtopping event occurred in October, and there were no significant differences in physicochemical values between the spring (11–13th of October) and neap (14–18th of October) tide conditions.

3.2 | Microbial Community Variability

3.2.1 | Microbial Community Structure Varies by Location Within the STE

The mean Shannon Diversity Index was 7.10 across all samples with a range of 4.08–8.78. Indices were significantly higher in porewater versus seawater samples (ANOVA, p value = 0.0037), indicating that microbial communities within the STE are more diverse than within the adjacent seawater surf.

Beta diversity was evaluated with canonical analysis of principal coordinates (CAP), which revealed three primary axes of microbial community variation at the ASV level (Figure 5). The first axis (CAP1) explained 13.7% of the variation and separated samples from Wells 1–3, Well 4, and seawater surf samples. Salinity and phosphate concentration were significantly correlated with CAP1 (scores = 0.819 and 0.714, respectively). CAP2 explained 10.8% of the variation and captured the overall depth gradient for all wells. Nitrate concentration and pH were significantly correlated with CAP2 (scores = 0.911 and 0.816, respectively). CAP3 explained 6.9% of the variation. Ammonia and DO concentrations were significantly correlated with CAP3 (scores = 0.595 and 0.510, respectively). CAP ordinations for each well revealed similar clusters by season and depth (Figure A4).

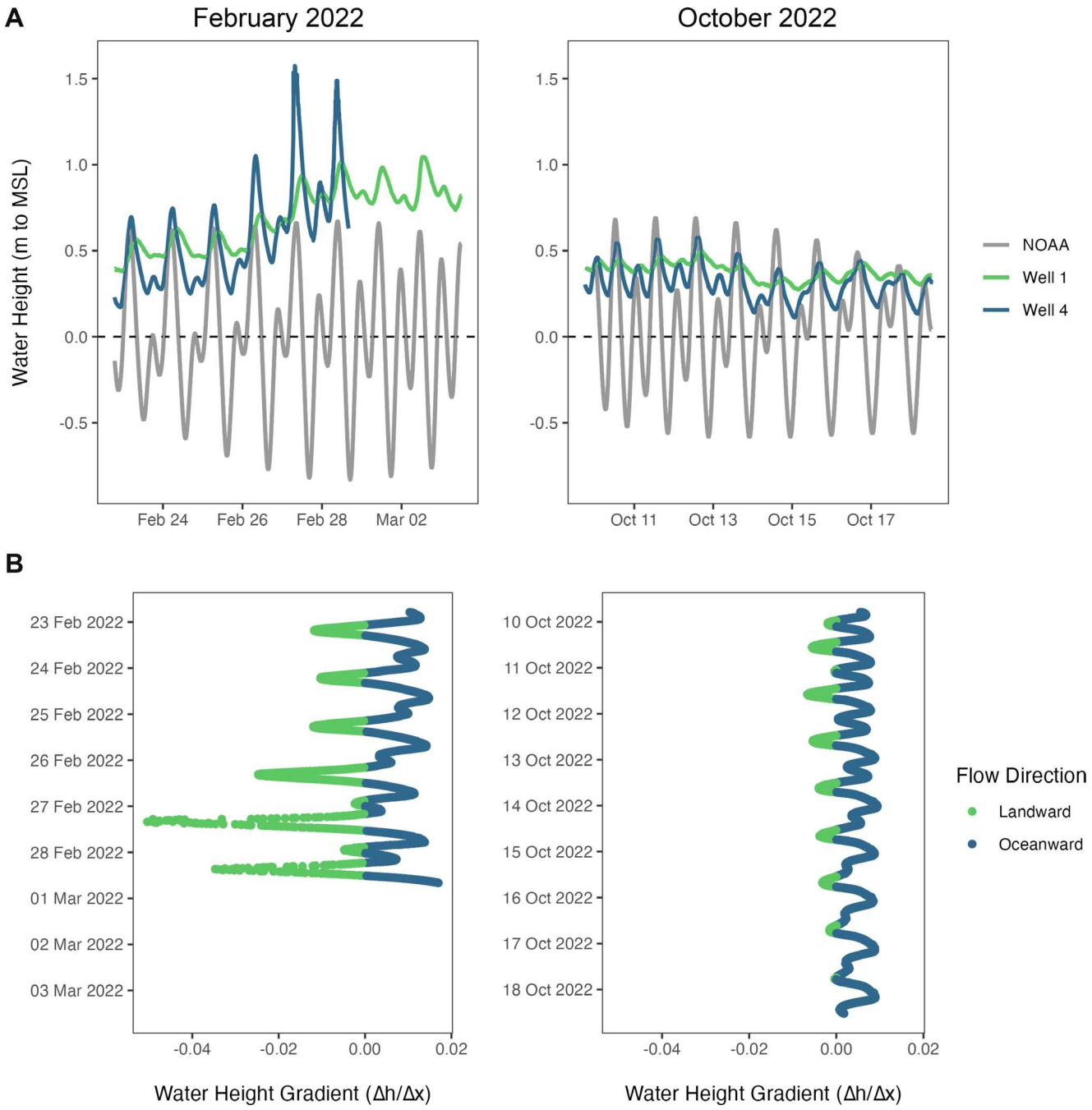

FIGURE 2 | Water height measurements relative to mean sea level (MSL) from Wells 1 and 4 during the sampling period for February and October 2022 (A). Predicted tide height (grey) from the nearest NOAA station (Bolinas Lagoon 9,414,958, labelled "NOAA") as a comparison. Well 4 logger was inundated by waves on 27 February and removed on 28 February 2022. In (B), the gradient in water height between Well 1 and Well 4. The gradient is calculated as the difference in water height relative to mean sea level (Δh) divided by the distance between Well 1 and Well 4 (Δx; 16.7 m in February and 19.7 m in October). When the water height at Well 1 was greater than Well 4, there was a positive gradient with oceanward flow, and vice versa.

Spatial and temporal variation of the microbial community was investigated using ANOSIM and PERMANOVA (Table 2; Figure A5). Similar to environmental measurements, microbial composition based on Bray–Curtis dissimilarity clustered according to region (shallow, intermediate, deep, Well 4, and seawater) within the STE. The region was significant (p value = 0.001) and explained 32.5% of the variation in community composition. Season and tidal regime were also significant (p value = 0.001), but explained only 5.9% and 2.0% of the variation, respectively.

There were challenges in testing community differences between seasons and tidal regimes. There were significant differences in dispersion between the season groups (PERMDISP, p value = 0.035), which can be conflated with compositional differences when utilizing distance-based significance tests (Anderson and Walsh 2013). Furthermore, the transition to spring tide in February co-occurred with the significant effect of overtopping (p value = 0.001) on community composition. Tidal regime for the October dataset alone was not significant (p value = 0.485).

TABLE 1 | Median values for select physicochemical measurements by region within the subterranean estuary. A total of 516 porewater and 25 seawater surf samples were collected over 9 days in February and 8 days in October of 2022.

	Wells 1–3				
	Shallow	**Intermediate**	**Deep**	**Well 4**	**Seawater**
Salinity (PSU)	2.5	1.3	6.0	14.5	32.8
Temperature (°C)	14.2	15.0	17.2	12.6	12.7
DO (μM)	179.7	114.5	139.7	203.9	279.4
pH	8.6	8.2	7.9	8.0	8.0
Nitrate (μM)	288.3	237.0	10.3	90.7	9.6
Nitrite (μM)	5.4	3.2	1.9	0.0	0.3
Ammonia (μM)	1.6	0.5	6.4	0.3	3.1
Phosphate (μM)	24.3	12.7	33.4	4.7	1.9
Cells ml^{-1} ($\times 10^5$)	5.6	4.8	4.5	2.2	17.6
DOC (μM)	588.8	534.4	478.5	159.2	85.8
Fpeak (RFU)	0.06	0.04	0.06	0.01	0.00
HIX	16.6	17.7	16.4	13.6	4.2

Abbreviations: DO = dissolved oxygen; DOC = dissolved organic carbon; HIX = humification index.

The effect of tide (H/L) on community composition was tested for the February dataset since H and L samples were collected. There was no significant difference (p value >0.05) between H and L for all the February samples together or for subsets of the February dataset based on region or tidal regime.

3.2.2 | Microbial Composition Varies With Gradients in Salinity, Inorganic Nitrogen, and Organic Carbon

The set of environmental variables with the highest correlation to microbial community composition included salinity, temperature, DO, nitrate, ammonia, phosphate, DOC, and HIX (Spearman's $\rho=0.685$, Table 3). The singular variable with the highest correlation was DOC (Spearman's $\rho=0.454$), while the two variables combined with the highest correlation were salinity and nitrate (Spearman's $\rho=0.572$). For various subsets of the full porewater dataset, salinity, DIN, DOC, Fpeak, and HIX were consistently strongly correlated with variations in the microbial community composition (Table A4).

3.2.3 | Taxa Responsible for Shifts in Microbial Community Structure

There were 63,344 total unique ASVs and 7,613,584 total reads in the full porewater and seawater dataset. Most ASVs were classified at the phylum or lower level; however, there were 3,570 ASVs (2.96% of total reads) assigned to Bacteria and 119 ASVs (0.09% of total reads) assigned to Archaea that were unclassified at the phylum level. The number of unclassified reads at the phylum level was disproportionately higher in the deep samples (4.53% unclassified bacteria and 0.30% unclassified archaea) despite having similar total read counts to other regions of the STE.

Proteobacteria, Nanoarchaeota, Verrucomicrobiota, Patescibacteria (Candidate Phyla Radiation, CPR), and Bacteroidota were relatively abundant and prevalent across all porewater samples. Respectively, these phyla represented 26.8%, 19.8%, 10.3%, 7.2%, and 5.8% of the total reads including both porewater and seawater samples (Figure A6).

Proteobacteria were relatively abundant in shallow porewater as well as seawater samples, with decreasing abundance deeper into the STE (Figure 6; Figure A7). The relative abundance of Proteobacteria was positively correlated with DO measurements (Spearman's $\rho=0.41$; p value <0.001, Figure A8). There were 8,482 total ASVs classified as Proteobacteria. Proteobacteria genera with the highest relative abundance included *Shewanella* in the shallow and intermediate depth samples, *Gallionella* in the deep samples, and SAR11 Clade Ia in the Well 4 and seawater samples.

Nanoarchaeota within the DPANN superphylum were relatively abundant in Well 4 samples with lower abundance in shallow porewater samples and seawater samples (Figure 6; Figure A9). The relative abundance of Nanoarchaeota was negatively correlated with nitrite, ammonia, and DOC (Spearman's $\rho=-0.42$, -0.45, -0.44, respectively; p values <0.001, Figure A8). There were 10,748 ASVs classified as Nanoarchaeota. All Nanoarchaeota ASVs were further classified in the order Woesearchaeales, a proposed DPANN phylum Woesearchaeota (Castelle et al. 2015). Despite their abundance (nearly 20% of all reads in the dataset), Nanoarchaeota ASVs were poorly classified with 61.5% unclassified finer than order Woesearchaeales and the remaining resembling assembled genomes at the family (GW2011_GWC1_47_15, SCGC AAA011-D5, SCGC AAA286-E23, CG1-02-57-44) or genus (AR15, AR20) level.

Verrucomicrobiota were particularly abundant in intermediate and deep porewater samples (Figure 6; Figure A9).

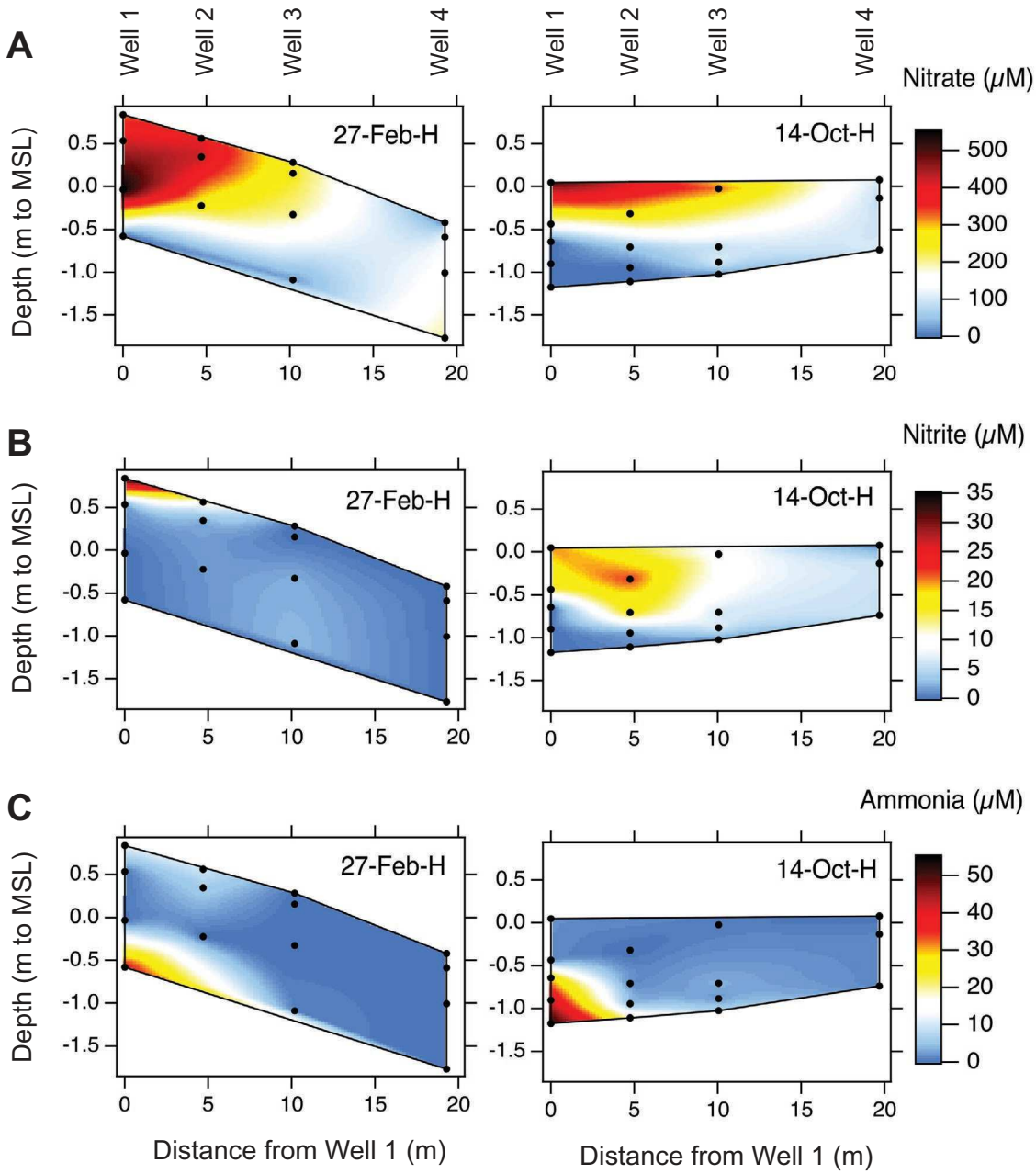

FIGURE 3 | Dissolved inorganic nitrogen concentrations across the beach transect highlighting depth structure within Wells 1–3 for February and October. Panels are distinguished by the date (day-month abbreviation) and tide (H = high-high). General features were consistent across dates and tides for nitrate (A), nitrite (B), and ammonia (C). Interpolation was performed using IGOR Pro (Wavemetrics). MSL = mean sea level.

Verrucomicrobiota relative abundance was negatively correlated with DO (Spearman's $\rho = -0.40$, p value < 0.001). There were 8,449 ASVs classified as Verrucomicrobiota. Of these ASVs, 6,110 were classified as class Omnitrophia, representing 82.1% of Verrucomicrobiota reads, now a separate phylum Omnitrophota also within the PVC superphylum. *Candidatus* Omnitrophus was the dominant genus representing 69.3% of all Verrucomicrobiota reads.

Patescibacteria, comprising the Candidate Phyla Radiation (CPR), had a fairly uniform distribution across porewater samples while mostly absent in seawater samples (Figure 6; Figure A9). CPR were negatively correlated with salinity and DO (Spearman's $\rho = -0.43$, -0.54, respectively, p values < 0.001). There were 6,685 ASVs classified as CPR. CPR were classified to the genus level for *Candidatus* Paceibacter (2.2% of all CPR reads), which were relatively abundant in deep samples. The majority of CPR reads were classified to the class level as primarily Parcubacteria (25.4%) and *Candidatus* Yanofskybacteria (11.9%).

Bacteroidota were relatively abundant in shallow porewater and seawater samples (Figure 6; Figure A9). Bacteroidota relative abundance was positively correlated with nitrate (Spearman's $\rho = 0.41$, p value < 0.001). There were 2,078 ASVs classified as Bacteroidota. Bacteroidota genera with the highest relative abundance included *Fluviicola* in the Well 4 as well as shallow and intermediate depth samples, *Maritimimonas* in the deep

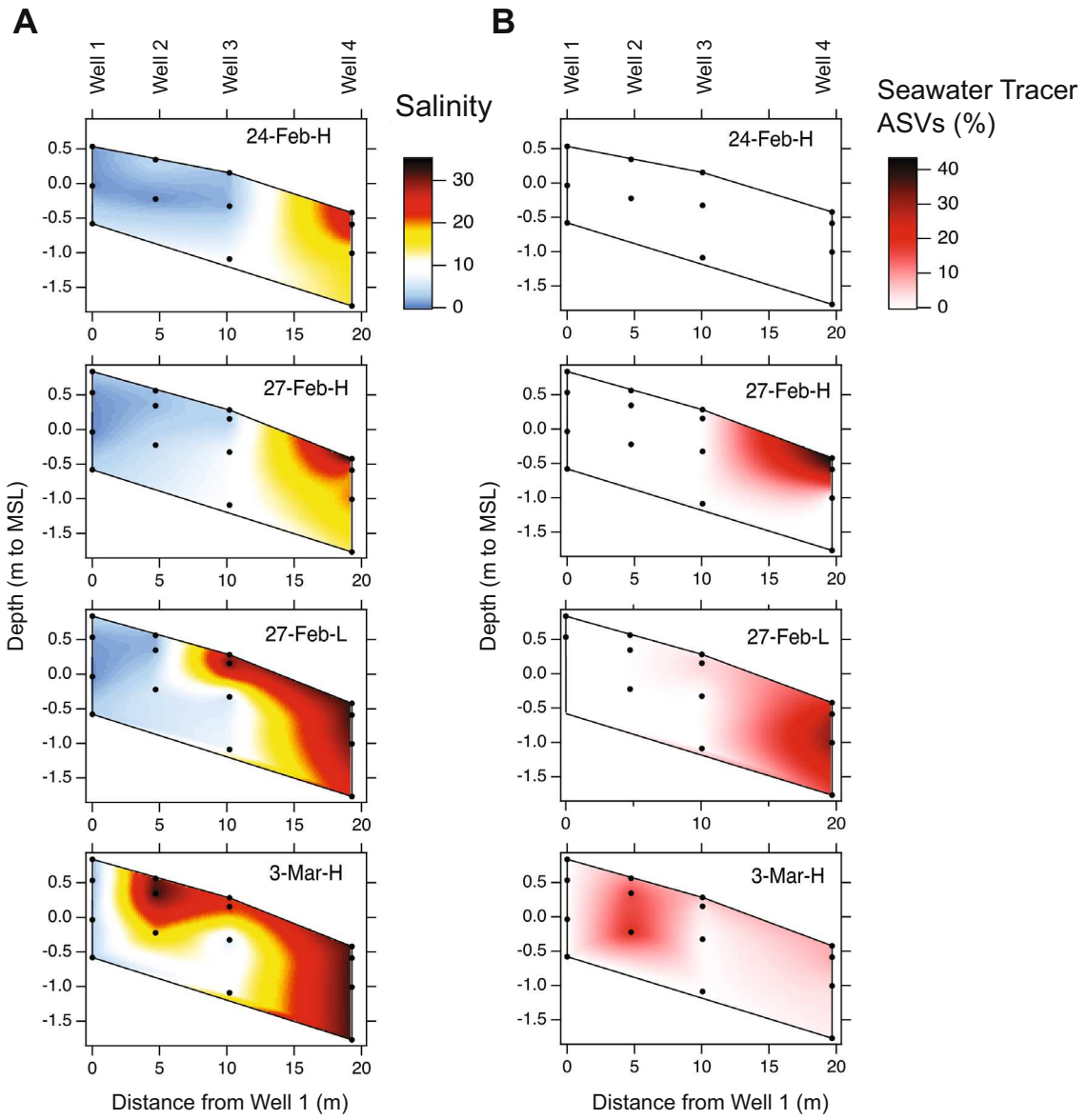

FIGURE 4 | Cross sections of the beach transect showing infiltrating seawater following the wave overtopping event at Well 4 during the 27 February high-high tide. Salinity (A) and percent seawater tracer amplicon sequence variants (ASVs) (B) across the beach transect for select dates and tides. Panels are distinguished by the date (day-month abbreviation) and tide (H = high-high and L = low-low). Percent seawater tracer ASVs was calculated as the sum of the reads assigned as seawater tracer ASVs divided by the total reads for each sample. Taxonomic identification of the ASVs is in the text. Interpolation was performed using IGOR Pro (Wavemetrics, Portland, OR). MSL = mean sea level.

samples, and members of the NS5 marine group in the family Flavobacteriaceae in the seawater samples.

3.2.4 | Taxonomic Indicators of STE Region

Phyla and ASVs enriched in each STE cluster region (shallow, intermediate, deep, Well 4, and seawater) were identified using DESeq. Based on log 2 fold change, Firmicutes had the highest enrichment in the shallow region, Methylomirabilota in the intermediate region, Campylobacterota in the deep region, Nanoarchaeota in Well 4, and Actinobacteriota in seawater (Table A5). There were 353 ASVs significantly enriched (adjusted p values <0.05) in the shallow, 345 in the intermediate, 181 in the deep, and 317 in the Well 4 STE regions with relative abundance over 0.01% of total reads. The top 10 most enriched ASVs from each region, based on the log 2 fold change relative to all other samples, are presented in Figure A10.

3.2.5 | Overtopping Surface Waves Impact Community Composition in the STE

There were 16 ASVs significantly enriched in seawater samples compared to porewater samples prior to February 27, when a wave set overtopped Well 4 and infiltrated the landward STE (Figure 4). These 16 ASVs were used as tracers of a seawater community within the porewater post February 27. They belonged to the genus *Amylibacter* (ASV 12), SAR11 Clade Ia (ASVs 8, 15, and 321), SAR86 clade (ASVs 42 and 90), SAR92

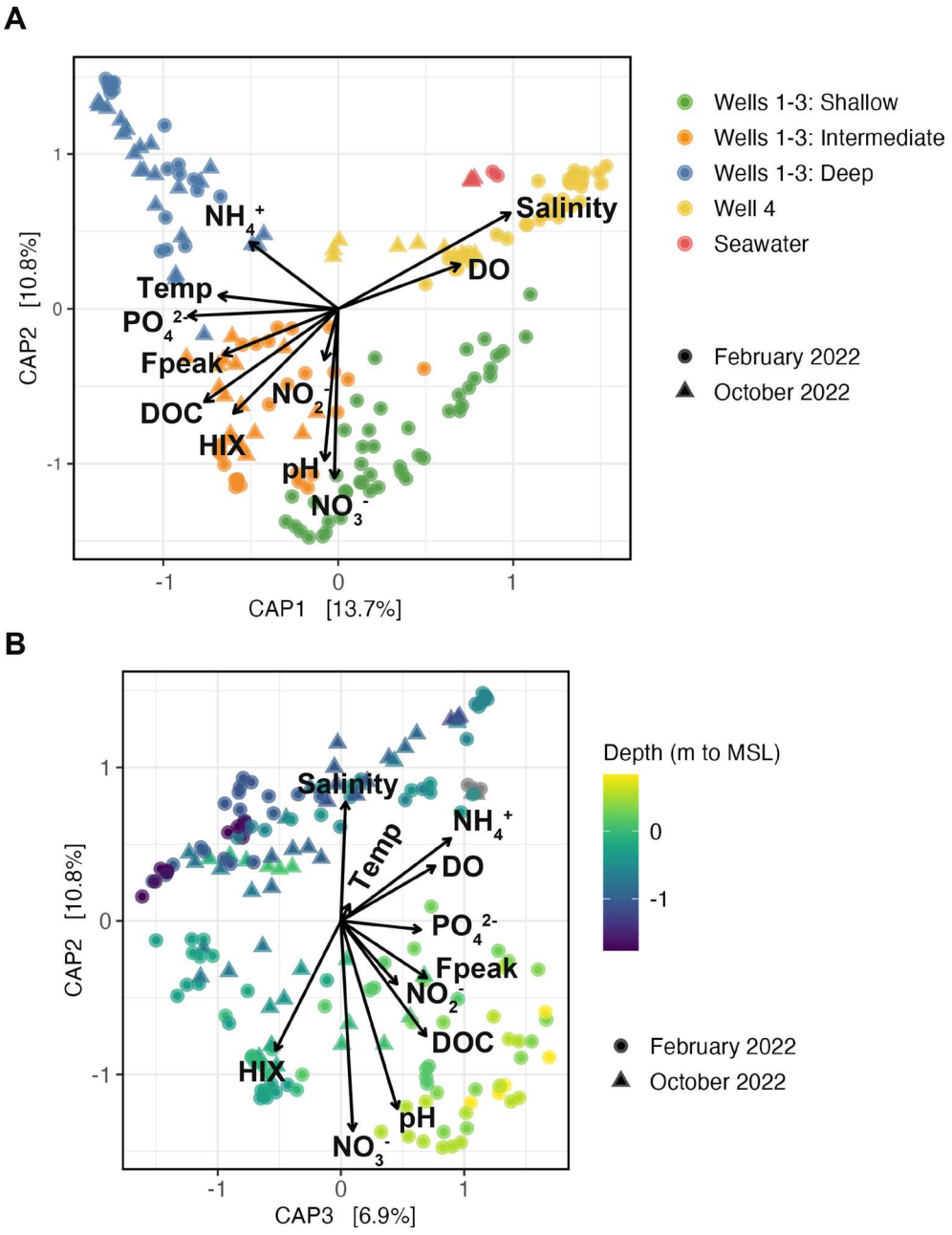

FIGURE 5 | Constrained analysis of principal coordinates (CAP) using the Bray–Curtis dissimilarity matrix of microbial ASV data and the reduced subset of environmental variables. Axes 1 and 2 (A) and axes 2 and 3 (B) are shown with the percent of variation explained on each axis. Samples are plotted as circles (February 2022) or triangles (October 2022). The color of each sample represents the region (A) or depth in meters to mean sea level (B). Grey samples (B) are seawater surf samples that were not subterranean. Temp = temperature; DO = dissolved oxygen; DOC = dissolved organic carbon; HIX = humification index; MSL = mean sea level.

clade (ASV 379), SUP05 cluster (ASVs 49 and 101), NS4 marine group (ASV 109), NS5 marine group (ASV 462), NS2b marine group (ASV 155), OM182 clade (ASV 188), OM60(NOR5) clade (ASV 992), *Planktomarina* (ASV 76), and *Synechococcus* CC9902 (ASV 926).

The initial detection of the wave overtopping impact on the STE microbial community occurred at the shallowest depths at Well 4 during the February 27 H tide (Figure 4; Figure A11; Figure A12). At this time, reads from seawater tracer ASVs alone comprised 42.1% of all reads within the shallowest Well 4 sample. There was a delayed impact of the seawater infiltrating deeper and horizontally reaching Well 2 by March 3 H tide. Reads from tracer ASVs reached 18.8% in the deepest Well 2 sample. Well 1 remained unaffected throughout the times sampled with seawater tracers reads $<1\%$. The relative abundance of seawater tracer ASVs declined after the initial delayed impact. This wave overtopping event and seawater infiltration disturbed the distinct separations of microbial communities by region within the Stinson Beach STE, but the effect was transient and minimal landward within the STE porewater.

TABLE 2 | Spatial and temporal variation of microbial community composition. The Bray–Curtis dissimilarity matrix was generated using ASV-level data for all porewater samples.

		Homogeneity of group dispersion (PERMDISP)		Analysis of similarities (ANOSIM)		Permutational analysis of variance (PERMANOVA)	
Explanatory variable	***n***	***F* statistic**	***p***	**Global *R***	***p***	***R*²**	***p***
Region (shallow, intermediate, deep, well 4)	178	0.560	0.649	0.829	0.001***	0.325	0.001***
Season (February, October)	178	4.524	0.035*	0.221	0.001***	0.059	0.001***
Tidal regime (spring, neap)	178	0.444	0.508	0.060	0.001***	0.020	0.001***
Overtopping (pre, post)	130[a]	0.103	0.756	0.062	0.014*	0.022	0.001***
Tide (H, L)	130[a]	0.017	0.909	−0.012	0.889	0.004	0.988

Note: *n* = number of observations; Significance codes: 0 '***' 0.001 '**' 0.01 '*' 0.05 '.' 0.1 ' ' 1.
[a]February dataset only.

4 | Discussion

The findings of this study provide important new insights into the spatial and temporal microbial dynamics in a STE that, to our knowledge, have not been observed at such fine resolution. We attempted to characterize how dynamic changes in hydrology and physicochemistry of the STE at various spatial and temporal scales affect the microbial community. To accomplish this, we collected 187 samples for V4 16S rRNA gene amplicon sequencing from 17 locations (4 wells each with 3–5 depths) and 13 time points spanning two seasons and several tidal conditions at the STE located at Stinson Beach, California, USA.

4.1 | Predominant Spatial Heterogeneity of the STE Environment and Microbial Community

Despite dynamic tidal variation across our sampling time points, there were temporally stable physicochemical gradients within the Stinson Beach STE. From the most landward to oceanward sampling wells, there were dramatic decreases in DIN, DOC, and fDOM metrics in addition to the increase in salinity. For example, concentrations of nitrate exceeded 500 μM in Wells 1–3 while rarely above 100 μM in Well 4 and 10 μM in seawater samples. Similarly, concentrations of DOC exceeded 900 μM in Wells 1–3 while rarely above 300 μM in Well 4 and 90 μM in seawater samples. There are likely physical and biological processes accounting for these discrepancies as meteoric groundwater mixes with seawater. For instance, in addition to dilution, denitrification could contribute to the decline in nitrate and DOC as nutrient-rich groundwater discharges to the ocean.

Overlayed with this horizontal structure from land to sea, there were distinct depth gradients within Wells 1–3. Shallow, fresher porewaters were enriched in nitrate, while deeper, saltier waters were enriched in ammonia. Intermediate depths represented a transition zone with occasional hotspots of high nitrite concentrations. At other STEs (Rogers and Casciotti 2010; Santoro 2010; Schutte et al. 2018; Wilson et al. 2023), these features have been associated with a shallow oxic layer and a deep anoxic salt wedge. While we did not detect anoxic conditions at any location, DIN distributions suggest possible transient anoxic conditions, anoxic microsites, or seepage from the deeper confined aquifer below.

The microbial community composition is neatly segregated by these spatial regions within the STE. The unique horizontal and vertical structure, within tens of meters and stable between seasons, could have important implications for microbially-mediated biogeochemical reactions and ecological interactions between microbial populations. For example, the high concentrations of DOC, DO and nitrate, and likely sulfate from seawater suggest sufficient, if not excessive availability of electron donors and acceptors for respiration. Additionally, nitrification and denitrification processes could contribute to the separation of nitrate and ammonia pools with depth.

Spatial heterogeneity also affects the distribution of microbial populations. Particular ASVs were associated with these regions within the STE, even within the same genus, suggesting that populations may be somewhat isolated. This spatial structure could be used as a baseline biomarker for changing conditions in subsequent assessments.

4.2 | Minimal Seasonal and Tidal Variation

Compared to spatial gradients, temporal variations had smaller effect sizes on the physicochemical and microbial community composition. On average, there were seasonal differences in porewater temperature and DIN concentrations as well as overall microbial community composition between February and October of 2022. Due to logistical constraints, samples from February and October were collected from slightly different depths, which might account for some of the observed differences. Other STE studies have found both seasonally resilient (Calvo-Martin et al. 2022; Degenhardt et al. 2020) and seasonally-variable communities (Chen et al. 2020; Jiang et al. 2020; McAllister et al. 2015; Wu et al. 2023). In this temperate location during a year with low rainfall, there was only an average 4°C warming in porewater between February and October. Further investigation should be conducted in locations with more dramatic climatic changes to capture the range of possible seasonal effects.

TABLE 3 | Correlation of physicochemical variables with microbial community composition as determined by BIOENV analysis. Strongly collinear variables were removed prior to analysis (see Figure A2).

Dataset	*n*	Best set of variables	Spearman's correlation (ρ)	Best singular variable	Spearman's correlation (ρ)	Best two variables	Spearman's correlation (ρ)
All porewater	178	Salinity, temperature, DO, pH, nitrate, nitrite, ammonia, phosphate, DOC, HIX	0.685	DOC	0.454	Salinity, nitrate	0.572
Shallow	46	Salinity, temperature, DO, pH, nitrate, nitrite, DOC, HIX	0.589	Salinity	0.435	Salinity, nitrite	0.554
Intermediate	44	Salinity, temperature, pH, nitrite, Fpeak	0.480	Nitrite	0.409	Salinity, temperature	0.451
Deep	43	Salinity, nitrite, ammonia	0.711	Nitrite	0.596	Salinity, nitrite	0.696
Well 4	45	Salinity, temperature, HIX	0.658	Salinity	0.569	Salinity, HIX	0.606

Abbreviations: *n* = number of observations; DO = dissolved oxygen; DOC = dissolved organic carbon; HIX = humification index.

There are no previous reports on the effects of tidal conditions on STE microbial communities. The physicochemical environment and microbial community composition were not significantly different between tidal regimes (spring/neap) or tides (H/L). The tidal influence may be muted within the Stinson Beach STE due to limited water displacement from tidal forcing. Using Darcy's Law and a hydraulic conductivity (K_h) of 3.85×10^{-4} m/s (de Sieyes et al. 2011) and a gradient range of 0.01–0.04 for a generous estimate of 6 h, the maximum tidal displacement during our sampling was estimated to be between 0.08 and 0.30 m. This displacement is much smaller than the 5–10 m between wells along the 20 m transect.

4.3 | Significant Impact of Overtopping Waves

Although tidally driven transport is limited, we captured the impact of overtopping waves significantly altering the physicochemical environment and transporting marine microbes into the STE. Following the overtopping event at Well 4 during the high-high tide on February 27, the salinity significantly increased while DIN, phosphate, and fDOM metrics significantly decreased within the STE. We identified 16 ASVs as tracers of this wave impact and subsequent infiltration. Tracer ASVs included marine members from the Flavobacteriaceae family (NS4, NS5, and NS2b), Rhodobacteraceae family (*Amylibacter, Planktomarina*), Pseudomonadales order (SAR86, SAR92, OM182, OM60), SAR11 clade, and *Synechococcus* cyanobacteria. Few studies (Boehm, Yamahara, and Sassoubre 2014; Russell, Yamahara, and Boehm 2012) have documented the transport of microbial cells through beach sands. Previous studies have noted the potential of inoculation from the marine environment into coastal aquifers (Adyasari et al. 2019; Chen et al. 2019; Unno et al. 2015). While Chen et al. (2019) proposed Oceanospirillales and Alteromonadaceae as potential indicators of seawater intrusion, Unno et al. (2015) proposed Rhodobacteraceae and Flavobacteriaceae similar to our own findings.

There are important ecological and biogeochemical ramifications of seawater infiltration due to overtopping waves. This event shows that porewater can be a conduit for the exchange of cellular material through the beach STE. The infiltrating seawater has very different chemical characteristics and microbial constituents, disrupting the spatial structure of the STE. Thus, these events can be used to study both connectivity and disturbance. Within a few tidal cycles at Stinson Beach, the 16 tracer ASVs alone comprised nearly 20% of the total microbial community within the landward Well 2 site. However, the impact was restricted from reaching Well 1 and deeper depths. Shallower depth communities are likely more connected to the ocean and potentially more resilient to these transient events. Wave overtopping events are more likely to occur during particular tidal regimes and times of the year, such as winter spring tides, when water levels are heightened. The impact of overtopping waves can be a lens to the near future as sea levels rise and storm surges become more intense due to climate changes.

Follow-up research to determine the activity of these transported cells, such as transcriptomics, will be necessary to fully characterise this impact and the impact of other stochastic events such as rainfall. Regardless, our observations confirm

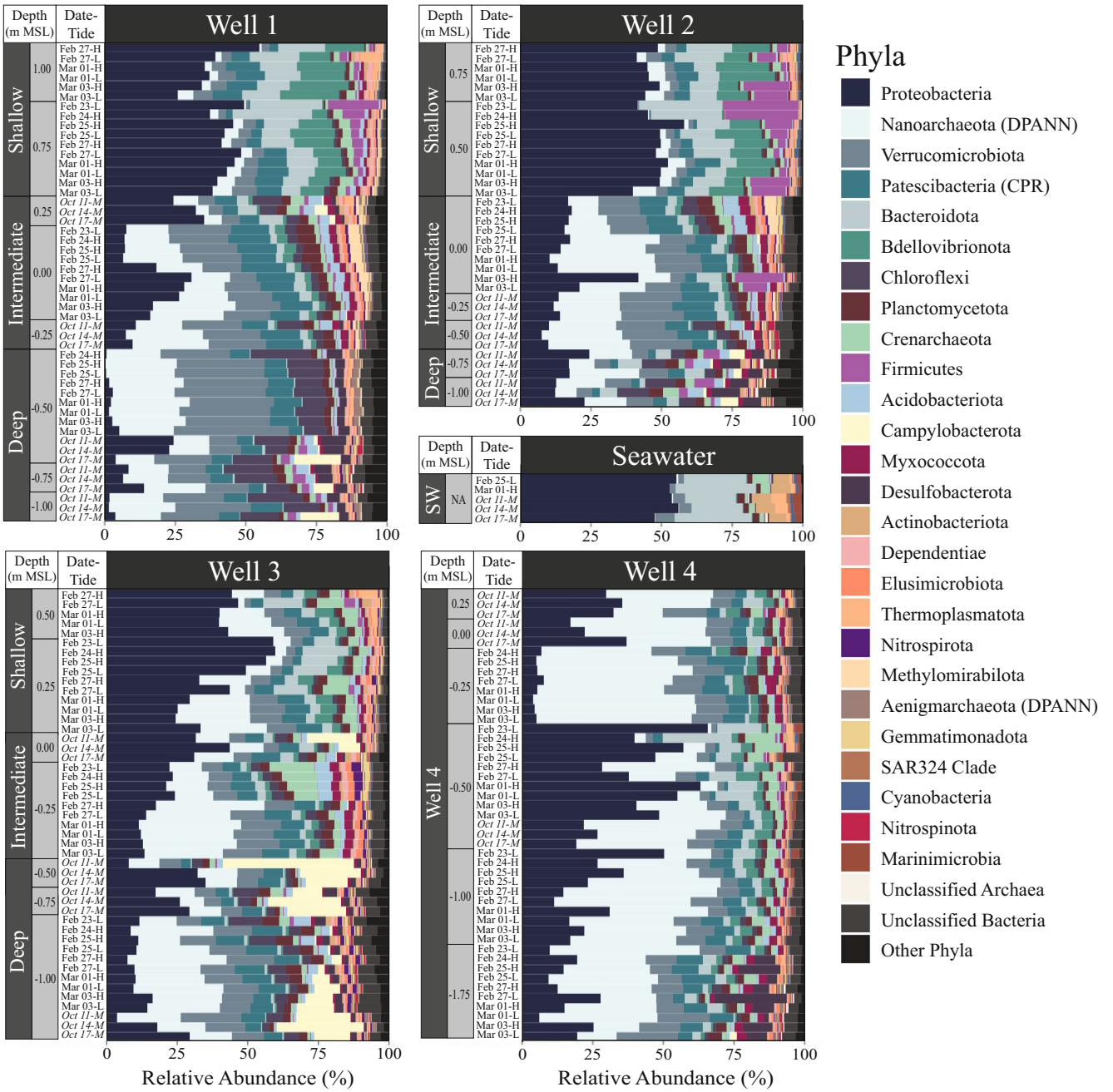

FIGURE 6 | Relative abundance of phyla for each porewater ($n = 182$) and seawater (SW) sample ($n = 5$). Replicate samples were not collected. Individual phyla displayed are over 0.16% of the total sequencing reads and ordered by contribution to total reads. These phyla represent 95% of total reads collectively and 26/80 of the total classified phyla. Other phyla are grouped into the "Other" category. Samples are sectioned into each well and binned by region (shallow, intermediate, deep, Well 4, or seawater). Within each bin, samples are ordered by depth (m to MSL) and then sequentially by date and tide. October samples are labelled in italics.

the transport of cellular material through the STE environment over a few days.

4.4 | Taxonomic Diversity Within the STE

Taxonomically, a notable portion of our ASVs and sequencing reads were unclassified at the phylum level, particularly in the deep samples. Groundwater aquifers have been shown to harbor a diversity of unknown taxa (Anantharaman et al. 2016; Castelle et al. 2013). Among the classified reads, Proteobacteria were relatively abundant as well as several phyla considered "ultrasmall". Patescibacteria (CPR), members of the DPANN radiation, Omnitrophota (previously within Verrucomicrobiota), and Actinomarinales have characteristically small cell sizes and reduced genomes (Castelle and Banfield 2018; Castelle et al. 2015; Dombrowski et al. 2019; López-Pérez et al. 2020; Sakai et al. 2022; Seymour et al. 2023). Previous STE studies have reported the presence of CPR (Adyasari et al. 2020; Ruiz-González et al. 2022), members of the DPANN superphylum (Adyasari et al. 2020; Calvo-Martin et al. 2022; Chen et al. 2019; Degenhardt et al. 2020; Ruiz-González et al. 2022), and

Omnitrophota (Adyasari et al. 2020; Calvo-Martin et al. 2022), but at lower relative abundances than found within our samples. Although it is possible that our methods of sampling porewater rather than sand selectively captured these taxa, Stinson Beach may also harbor uniquely abundant populations of these "ultrasmall" taxa.

In other high-energy sandy beach STEs, the microbial community was comprised of a core set of abundant generalists, independent of transect location and sampling depth, that were persistent over seasons within beach sands (Degenhardt et al. 2020). Calvo-Martin et al. (2022) noted the ubiquity of abundant cosmopolitan taxa between two beaches with seasonally-resilient communities specific to their shallow (0.29 m relative to the sand surface) and deep (1.78 m) porewater samples. These cosmopolitan taxa within the Proteobacteria, Thaumarchaeota (now Nitrososphaerota), Nanoarchaeaeota, and Chloroflexi phyla were similar to those found across intertidal beach sand samples spanning the California coast (Boehm, Yamahara, and Sassoubre 2014). While the microbial members present at the Stinson Beach STE were taxonomically similar to those identified previously, the community was heterogeneous by location and temporally variable.

5 | Conclusions

This research is the first to target daily and sub-daily tidal variation of the microbial community within a STE. Our results highlight three main findings regarding the structure of the microbial community in the high-energy, sandy beach STE: (1) the region within the STE was a primary determinant of community composition, while transitions between high and low tides had no discernible impact; (2) salinity, DIN, and DOC were significant environmental correlates of community composition, with additional variation explained by DOM quality, particularly the humification index (HIX); and (3) transport of microbial cells in the porewater is possible via the disturbance of surface waves and subsequent infiltration of seawater. The abundance of completely unclassified bacteria and archaea, as well as "ultrasmall" taxa, warrants further investigation. These findings have important implications for the impacts of sea level rise, which are projected to fully inundate Stinson Beach by 2100, as well as the capacity for the beach aquifer to process pollutants from human activities. Follow-up research using techniques targeting specific metabolic capabilities, ecological roles, and activity measurements will further enhance our understanding of these unique subterranean communities.

Author Contributions

Jessica A. Bullington: formal analysis, investigation, writing – original draft, visualization, funding acquisition. **Kathryn Langenfeld:** formal analysis, writing – original draft, visualization, investigation. **Jacob R. Phaneuf:** investigation, writing – review and editing. **Alexandria B. Boehm:** conceptualization, resources, visualization, writing – review and editing, project administration, supervision, funding acquisition. **Christopher A. Francis:** conceptualization, resources, writing – review and editing, supervision, project administration, funding acquisition.

Acknowledgements

We thank the many volunteers who assisted with field sample collection, including Meghan Shea, Claire Anderson, Ryan Searcy, Mengyang Zhang, Lauren Kennedy, Ken Czapla, Ben Shapero, Amanda Bidwell, Katelin Scheuerman, Ian Morris, and Nimisha Singla, and those who helped with sample processing, including Sean Swift, Skye Inn, Camila Van Oost, and Maria Ridgeway-Elsner. We also thank Lily Chang for conducting the beach slope surveys, Craig Nelson for fDOM resources, Bennett Kapili for a sequencing analysis template, Anne Dekas for microscope access, and Chris Kelley for coordination with the Stinson Beach County Water District. Samples were collected under the National Marine Sanctuary Permit GFNMS-2020-006 and Marin County Parks permit 22024. This research was funded by NSF 'Understanding the Rules of Life: Microbiome Theory and Mechanisms' (URoL:MTM) Award #2024504 to A.B.B. and C.A.F. Additional funding was provided by a Stanford McGee and Levorsen Research Grant and an ARCO Stanford Graduate Fellowship to J.A.B.

Conflicts of Interest

The authors declare no conflicts of interest.

Data Availability Statement

Data and statistical analyses are publicly available on the Stanford Digital Repository: https://doi.org/10.25740/zm209tn5260 and GitHub repository: https://github.com/jessicabullington/stinson-STE-microbiome.git. Amplicon sequences are available through NCBI SRA BioProject PRJNA1171120: https://www.ncbi.nlm.nih.gov/bioproject/PRJNA1171120.

References

Adyasari, D., C. Hassenrück, D. Montiel, and N. Dimova. 2020. "Microbial Community Composition Across a Coastal Hydrological System Affected by Submarine Groundwater Discharge (SGD)." *PLoS One* 15, no. 6: e0235235. https://doi.org/10.1371/journal.pone.0235235.

Adyasari, D., C. Hassenrück, T. Oehler, A. Sabdaningsih, and N. Moosdorf. 2019. "Microbial Community Structure Associated With Submarine Groundwater Discharge in Northern Java (Indonesia)." *Science of the Total Environment* 689: 590–601. https://doi.org/10.1016/j.scitotenv.2019.06.193.

Anantharaman, K., C. T. Brown, L. A. Hug, et al. 2016. "Thousands of Microbial Genomes Shed Light on Interconnected Biogeochemical Processes in an Aquifer System." *Nature Communications* 7: 13219. https://doi.org/10.1038/ncomms13219.

Anderson, M. J., and D. C. I. Walsh. 2013. "PERMANOVA, ANOSIM, and the Mantel Test in the Face of Heterogeneous Dispersions: What Null Hypothesis Are You Testing?" *Ecological Monographs* 83, no. 4: 557–574. https://doi.org/10.1890/12-2010.1.

Anschutz, P., T. Smith, A. Mouret, et al. 2009. "Tidal Sands as Biogeochemical Reactors." *Estuarine, Coastal and Shelf Science* 84, no. 1: 84–90. https://doi.org/10.1016/j.ecss.2009.06.015.

Archana, A., C. A. Francis, and A. B. Boehm. 2021. "The Beach Aquifer Microbiome: Research Gaps and Data Needs." *Frontiers in Environmental Science* 9: 653568. https://doi.org/10.3389/fenvs.2021.653568.

Boehm, A. B., K. M. Yamahara, and L. M. Sassoubre. 2014. "Diversity and Transport of Microorganisms in Intertidal Sands of the California Coast." *Applied and Environmental Microbiology* 80, no. 13: 3943–3951. https://doi.org/10.1128/AEM.00513-14.

Bower, C. E., and T. Holm-Hansen. 1980. "A Salicylate–Hypochlorite Method for Determining Ammonia in Seawater." *Canadian Journal of Fisheries and Aquatic Sciences* 37, no. 5: 794–798. https://doi.org/10.1139/f80-106.

Brown, A. C., and A. McLachlan. 2002. "Sandy Shore Ecosystems and the Threats Facing Them: Some Predictions for the Year 2025." *Environmental Conservation* 29, no. 1: 62–77. https://doi.org/10.1017/S037689290200005X.

Burdige, D. J., S. W. Kline, and W. Chen. 2004. "Fluorescent Dissolved Organic Matter in Marine Sediment Pore Waters." *Marine Chemistry* 89, no. 1: 289–311. https://doi.org/10.1016/j.marchem.2004.02.015.

Callahan, B. J., P. J. McMurdie, M. J. Rosen, A. W. Han, A. J. A. Johnson, and S. P. Holmes. 2016. "DADA2: High-Resolution Sample Inference From Illumina Amplicon Data." *Nature Methods* 13, no. 7: 581–583. https://doi.org/10.1038/nmeth.3869.

Calvo-Martin, E., E. Teira, X. A. Álvarez-Salgado, et al. 2022. "On the Hidden Diversity and Niche Specialization of the Microbial Realm of Subterranean Estuaries." *Environmental Microbiology* 24, no. 12: 5859–5881. https://doi.org/10.1111/1462-2920.16160.

Castelle, C. J., and J. F. Banfield. 2018. "Major New Microbial Groups Expand Diversity and Alter Our Understanding of the Tree of Life." *Cell* 172, no. 6: 1181–1197. https://doi.org/10.1016/j.cell.2018.02.016.

Castelle, C. J., L. A. Hug, K. C. Wrighton, et al. 2013. "Extraordinary Phylogenetic Diversity and Metabolic Versatility in Aquifer Sediment." *Nature Communications* 4: 2120. https://doi.org/10.1038/ncomms3120.

Castelle, C. J., K. C. Wrighton, B. C. Thomas, et al. 2015. "Genomic Expansion of Domain Archaea Highlights Roles for Organisms From New Phyla in Anaerobic Carbon Cycling." *Current Biology* 25, no. 6: 690–701. https://doi.org/10.1016/j.cub.2015.01.014.

Chen, X., Q. Ye, J. Du, and J. Zhang. 2019. "Bacterial and Archaeal Assemblages From Two Size Fractions in Submarine Groundwater Near an Industrial Zone." *Watermark* 11: 1261. https://doi.org/10.3390/w11061261.

Chen, X., Q. Ye, C. J. Sanders, J. Du, and J. Zhang. 2020. "Bacterial-Derived Nutrient and Carbon Source-Sink Behaviors in a Sandy Beach Subterranean Estuary." *Marine Pollution Bulletin* 160: 111570. https://doi.org/10.1016/j.marpolbul.2020.111570.

Clarke, K., and M. Ainsworth. 1993. "A Method of Linking Multivariate Community Structure to Environmental Variables." *Marine Ecology Progress Series* 92: 205–219. https://doi.org/10.3354/meps092205.

Coble, P. G. 1996. "Characterization of Marine and Terrestrial DOM in Seawater Using Excitation-Emission Matrix Spectroscopy." *Marine Chemistry* 51, no. 4: 325–346. https://doi.org/10.1016/0304-4203(95)00062-3.

Coble, P. G. 2007. "Marine Optical Biogeochemistry: The Chemistry of Ocean Color." *Chemical Reviews* 107, no. 2: 402–418. https://doi.org/10.1021/cr050350+.

Cooper, J. A. G., G. Masselink, G. Coco, et al. 2020. "Sandy Beaches Can Survive Sea-Level Rise." *Nature Climate Change* 10, no. 11: 993–995. https://doi.org/10.1038/s41558-020-00934-2.

Davis, N. M., D. M. Proctor, S. P. Holmes, D. A. Relman, and B. J. Callahan. 2018. "Simple Statistical Identification and Removal of Contaminant Sequences in Marker-Gene and Metagenomics Data." *Microbiome* 6, no. 1: 226. https://doi.org/10.1186/s40168-018-0605-2.

de Sieyes, N. R., K. M. Yamahara, B. A. Layton, E. H. Joyce, and A. B. Boehm. 2008. "Submarine Discharge of Nutrient-Enriched Fresh Groundwater at Stinson Beach, California Is Enhanced During Neap Tides." *Limnology and Oceanography* 53, no. 4: 1434–1445. https://doi.org/10.4319/lo.2008.53.4.1434.

de Sieyes, N. R., K. M. Yamahara, A. Paytan, and A. B. Boehm. 2011. "Submarine Groundwater Discharge to a High-Energy Surf Zone at Stinson Beach, California, Estimated Using Radium Isotopes." *Estuaries and Coasts* 34, no. 2: 256–268. https://doi.org/10.1007/s12237-010-9305-2.

Defeo, O., A. McLachlan, D. S. Schoeman, et al. 2009. "Threats to Sandy Beach Ecosystems: A Review." *Estuarine, Coastal and Shelf Science* 81, no. 1: 1–12. https://doi.org/10.1016/j.ecss.2008.09.022.

Degenhardt, J., L. Dlugosch, J. Ahrens, M. Beck, H. Waska, and B. Engelen. 2020. "Seasonal Dynamics of Microbial Diversity at a Sandy High Energy Beach Reveal a Resilient Core Community." *Frontiers in Marine Science* 7: 573570. https://doi.org/10.3389/fmars.2020.573570.

Degenhardt, J., S. Khodami, F. Milke, H. Waska, B. Engelen, and P. Martinez Arbizu. 2021. "The Three Domains of Life Within the Discharge Area of a Shallow Subterranean Estuary at a High Energy Beach." *Frontiers in Environmental Science* 9: 642098. https://doi.org/10.3389/fenvs.2021.642098.

Dixon, P. 2003. "VEGAN, a Package of R Functions for Community Ecology." *Journal of Vegetation Science* 14, no. 6: 927–930. https://doi.org/10.1111/j.1654-1103.2003.tb02228.x.

Dombrowski, N., J.-H. Lee, T. A. Williams, P. Offre, and A. Spang. 2019. "Genomic Diversity, Lifestyles and Evolutionary Origins of DPANN Archaea." *FEMS Microbiology Letters* 366, no. 2: fnz008. https://doi.org/10.1093/femsle/fnz008.

Hernes, P. J., B. A. Bergamaschi, R. S. Eckard, and R. G. M. Spencer. 2009. "Fluorescence-Based Proxies for Lignin in Freshwater Dissolved Organic Matter." *Journal of Geophysical Research: Biogeosciences* 114, no. G4: G00F03. https://doi.org/10.1029/2009JG000938.

Heiss, J. W., and H. A. Michael. 2014. "Saltwater-Freshwater Mixing Dynamics in a Sandy Beach Aquifer Over Tidal, Spring-Neap, and Seasonal Cycles." *Water Resources Research* 50, no. 8: 6747–6766. https://doi.org/10.1002/2014wr015574.

Hong, Y., J. Wu, S. Wilson, and B. Song. 2019. "Vertical Stratification of Sediment Microbial Communities Along Geochemical Gradients of a Subterranean Estuary Located at the Gloucester Beach of Virginia, United States." *Frontiers in Microbiology* 9: 3343. https://doi.org/10.3389/fmicb.2018.03343.

Huber, W., A. von Heydebreck, H. Sültmann, A. Poustka, and M. Vingron. 2002. "Variance Stabilization Applied to Microarray Data Calibration and to the Quantification of Differential Expression." *Bioinformatics* 18, no. suppl_1: S96–S104. https://doi.org/10.1093/bioinformatics/18.suppl_1.S96.

Huguet, A., L. Vacher, S. Relexans, S. Saubusse, J. M. Froidefond, and E. Parlanti. 2009. "Properties of Fluorescent Dissolved Organic Matter in the Gironde Estuary." *Organic Geochemistry* 40, no. 6: 706–719. https://doi.org/10.1016/j.orggeochem.2009.03.002.

Hussain, M., R. Shamey, D. Hinks, A. El-Shafei, and S. I. Ali. 2012. "Synthesis of Novel Stilbene-Alkoxysilane Fluorescent Brighteners, and Their Performance on Cotton Fiber as Fluorescent Brightening and Ultraviolet Absorbing Agents." *Dyes and Pigments* 92, no. 3: 1231–1240. https://doi.org/10.1016/j.dyepig.2011.06.034.

Jiang, S., Y. Zhang, J. Jin, et al. 2020. "Organic Carbon in a Seepage Face of a Subterranean Estuary: Turnover and Microbial Interrelations." *Science of the Total Environment* 725: 138220. https://doi.org/10.1016/j.scitotenv.2020.138220.

Kolde, R. 2019. "Pheatmap: Pretty Heatmaps. R Package Version 1.0.12." https://CRAN.R-project.org/package=pheatmap.

Lecher, A. L., and K. R. M. Mackey. 2018. "Synthesizing the Effects of Submarine Groundwater Discharge on Marine Biota." *Hydrology* 5, no. 4: 60. https://doi.org/10.3390/hydrology5040060.

Lee, Y.-W., G. Kim, W.-A. Lim, and D.-W. Hwang. 2010. "A Relationship Between Submarine Groundwater Borne Nutrients Traced by Ra Isotopes and the Intensity of Dinoflagellate Red-Tides Occurring in the Southern Sea of Korea." *Limnology and Oceanography* 55, no. 1: 1–10. https://doi.org/10.4319/lo.2010.55.1.0001.

Liefer, J. D., H. L. MacIntyre, L. Novoveská, W. L. Smith, and C. P. Dorsey. 2009. "Temporal and Spatial Variability in *Pseudo-Nitzschia* Spp. in Alabama Coastal Waters: A "Hot Spot" Linked to Submarine Groundwater Discharge?" *Harmful Algae* 8, no. 5: 706–714. https://doi.org/10.1016/j.hal.2009.02.003.

Love, M. I., W. Huber, and S. Anders. 2014. "Moderated Estimation of Fold Change and Dispersion for RNA-Seq Data With DESeq2." *Genome Biology* 15, no. 12: 550. https://doi.org/10.1186/s13059-014-0550-8.

López-Pérez, M., J. M. Haro-Moreno, J. Iranzo, and F. Rodriguez-Valera. 2020. "Genomes of the "Candidatus Actinomarinales" Order: Highly Streamlined Marine Epipelagic Actinobacteria." *MSystems* 5, no. 6: 10–1128. https://doi.org/10.1128/msystems.01041-20.

Luijendijk, A., G. Hagenaars, R. Ranasinghe, F. Baart, G. Donchyts, and S. Aarninkhof. 2018. "The State of the World's Beaches." *Scientific Reports* 8, no. 1: 6641. https://doi.org/10.1038/s41598-018-24630-6.

McAllister, S. M., J. M. Barnett, J. W. Heiss, et al. 2015. "Dynamic Hydrologic and Biogeochemical Processes Drive Microbially Enhanced Iron and Sulfur Cycling Within the Intertidal Mixing Zone of a Beach Aquifer." *Limnology and Oceanography* 60, no. 1: 329–345. https://doi.org/10.1002/lno.10029.

McKnight, D. M., E. W. Boyer, P. K. Westerhoff, P. T. Doran, T. Kulbe, and D. T. Andersen. 2001. "Spectrofluorometric Characterization of Dissolved Organic Matter for Indication of Precursor Organic Material and Aromaticity." *Limnology and Oceanography* 46, no. 1: 38–48. https://doi.org/10.4319/lo.2001.46.1.0038.

McMurdie, P. J., and S. Holmes. 2013. "Phyloseq: An R Package for Reproducible Interactive Analysis and Graphics of Microbiome Census Data." *PLoS One* 8, no. 4: e61217. https://doi.org/10.1371/journal.pone.0061217.

McMurdie, P. J., and S. Holmes. 2014. "Waste Not, Want Not: Why Rarefying Microbiome Data Is Inadmissible." *PLoS Computational Biology* 10, no. 4: e1003531. https://doi.org/10.1371/journal.pcbi.1003531.

Moore, W. S. 1999. "The Subterranean Estuary: A Reaction Zone of Ground Water and Sea Water." *Marine Chemistry* 65, no. 1: 111–125. https://doi.org/10.1016/S0304-4203(99)00014-6.

Moore, W. S., C. Benitez-Nelson, C. Schutte, et al. 2024. "SGD-OD: Investigating the Potential Oxygen Demand of Submarine Groundwater Discharge in Coastal Systems." *Scientific Reports* 14, no. 1: 9249. https://doi.org/10.1038/s41598-024-59229-7.

Murphy, J., and J. P. Riley. 1962. "A Modified Single Solution Method for the Determination of Phosphate in Natural Waters." *Analytica Chimica Acta* 27: 31–36. https://doi.org/10.1016/S0003-2670(00)88444-5.

Nagul, E. A., I. D. McKelvie, P. Worsfold, and S. D. Kolev. 2015. "The Molybdenum Blue Reaction for the Determination of Orthophosphate Revisited: Opening the Black Box." *Analytica Chimica Acta* 890: 60–82. https://doi.org/10.1016/j.aca.2015.07.030.

Nelson, C. E., M. J. Donahue, H. Dulaiova, et al. 2015. "Fluorescent Dissolved Organic Matter as a Multivariate Biogeochemical Tracer of Submarine Groundwater Discharge in Coral Reef Ecosystems." *Marine Chemistry* 177: 232–243. https://doi.org/10.1016/j.marchem.2015.06.026.

Oksanen, J., G. Simpson, F. Blanchet, et al. 2022. "Vegan: Community Ecology Package. R Package Version 2.6–4." https://CRAN.R-project.org/package=vegan.

Quast, C., E. Pruesse, P. Yilmaz, et al. 2013. "The SILVA Ribosomal RNA Gene Database Project: Improved Data Processing and Web-Based Tools." *Nucleic Acids Research* 41, no. D1: D590–D596. https://doi.org/10.1093/nar/gks1219.

R Core Team. 2023. *R: A Language and Environment for Statistical Computing*. Vienna, Austria: R Foundation for Statistical Computing. https://www.R-project.org/.

Robinson, C., L. Li, and D. A. Barry. 2007. "Effect of Tidal Forcing on a Subterranean Estuary." *Advances in Water Resources* 30, no. 4: 851–865. https://doi.org/10.1016/j.advwatres.2006.07.006.

Robinson, C. E., P. Xin, I. R. Santos, M. A. Charette, L. Li, and D. A. Barry. 2018. "Groundwater Dynamics in Subterranean Estuaries of Coastal Unconfined Aquifers: Controls on Submarine Groundwater Discharge and Chemical Inputs to the Ocean." *Advances in Water Resources* 115: 315–331. https://doi.org/10.1016/j.advwatres.2017.10.041.

Rocha, C., C. E. Robinson, I. R. Santos, H. Waska, H. A. Michael, and H. J. Bokuniewicz. 2021. "A Place for Subterranean Estuaries in the Coastal Zone." *Estuarine, Coastal and Shelf Science* 250: 107167. https://doi.org/10.1016/j.ecss.2021.107167.

Rogers, D. R., and K. L. Casciotti. 2010. "Abundance and Diversity of Archaeal Ammonia Oxidizers in a Coastal Groundwater System." *Applied and Environmental Microbiology* 76, no. 24: 7938–7948. https://doi.org/10.1128/AEM.02056-09.

Ruiz-González, C., V. Rodellas, and J. Garcia-Orellana. 2021. "The Microbial Dimension of Submarine Groundwater Discharge: Current Challenges and Future Directions." *FEMS Microbiology Reviews* 45, no. 5: fuab010. https://doi.org/10.1093/femsre/fuab010.

Ruiz-González, C., L. Rodríguez-Pie, O. Maister, et al. 2022. "High Spatial Heterogeneity and Low Connectivity of Bacterial Communities Along a Mediterranean Subterranean Estuary." *Molecular Ecology* 31, no. 22: 5745–5764. https://doi.org/10.1111/mec.16695.

Russell, T. L., K. M. Yamahara, and A. B. Boehm. 2012. "Mobilization and Transport of Naturally Occurring Enterococci in Beach Sands Subject to Transient Infiltration of Seawater." *Environmental Science & Technology* 46, no. 11: 5988–5996. https://doi.org/10.1021/es300408z.

Sáenz, J. P., E. C. Hopmans, D. Rogers, et al. 2012. "Distribution of Anaerobic Ammonia-Oxidizing Bacteria in a Subterranean Estuary." *Marine Chemistry* 136–137: 7–13. https://doi.org/10.1016/j.marchem.2012.04.004.

Sakai, H. D., N. Nur, S. Kato, et al. 2022. "Insight Into the Symbiotic Lifestyle of DPANN Archaea Revealed by Cultivation and Genome Analyses." *Proceedings of the National Academy of Sciences* 119, no. 3: e2115449119. https://doi.org/10.1073/pnas.2115449119.

Santoro, A. E. 2010. "Microbial Nitrogen Cycling at the Saltwater–Freshwater Interface." *Hydrogeology Journal* 18, no. 1: 187–202. https://doi.org/10.1007/s10040-009-0526-z.

Santoro, A. E., A. B. Boehm, and C. A. Francis. 2006. "Denitrifier Community Composition Along a Nitrate and Salinity Gradient in a Coastal Aquifer." *Applied and Environmental Microbiology* 72, no. 3: 2102–2109. https://doi.org/10.1128/AEM.72.3.2102-2109.2006.

Santoro, A. E., C. A. Francis, N. R. De Sieyes, and A. B. Boehm. 2008. "Shifts in the Relative Abundance of Ammonia-Oxidizing Bacteria and Archaea Across Physicochemical Gradients in a Subterranean Estuary." *Environmental Microbiology* 10, no. 4: 1068–1079. https://doi.org/10.1111/j.1462-2920.2007.01547.x.

Schutte, C. A., A. M. Wilson, T. Evans, W. S. Moore, and S. B. Joye. 2018. "Deep Oxygen Penetration Drives Nitrification in Intertidal Beach Sands." *Limnology and Oceanography* 63, no. S1: S193–S208. https://doi.org/10.1002/lno.10731.

Seymour, C. O., M. Palmer, E. D. Becraft, et al. 2023. "Hyperactive Nanobacteria With Host-Dependent Traits Pervade Omnitrophota." *Nature Microbiology* 8, no. 4: 727–744. https://doi.org/10.1038/s41564-022-01319-1.

Somerfield, P. J., K. R. Clarke, and R. N. Gorley. 2021. "Analysis of Similarities (ANOSIM) for 2-Way Layouts Using a Generalised ANOSIM Statistic, With Comparative Notes on Permutational Multivariate Analysis of Variance (PERMANOVA)." *Austral Ecology* 46, no. 6: 911–926. https://doi.org/10.1111/aec.13059.

Stedmon, C. A., and S. Markager. 2005. "Resolving the Variability in Dissolved Organic Matter Fluorescence in a Temperate Estuary and Its Catchment Using PARAFAC Analysis." *Limnology and Oceanography* 50, no. 2: 686–697. https://doi.org/10.4319/lo.2005.50.2.0686.

Suzuki, Y., Y. Sugimura, and T. Itoh. 1985. "A Catalytic Oxidation Method for the Determination of Total Nitrogen Dissolved in Seawater."

Marine Chemistry 16, no. 1: 83–97. https://doi.org/10.1016/0304-4203(85)90029-5.

Suzuki, Y., E. Tanoue, and H. Ito. 1992. "A High-Temperature Catalytic Oxidation Method for the Determination of Dissolved Organic Carbon in Seawater: Analysis and Improvement." *Deep Sea Research Part A. Oceanographic Research Papers* 39, no. 2: 185–198. https://doi.org/10.1016/0198-0149(92)90104-2.

Unno, T., J. Kim, Y. Kim, et al. 2015. "Influence of Seawater Intrusion on Microbial Communities in Groundwater." *Science of the Total Environment* 532: 337–343. https://doi.org/10.1016/j.scitotenv.2015.05.111.

Vousdoukas, M. I., R. Ranasinghe, L. Mentaschi, et al. 2020. "Sandy Coastlines Under Threat of Erosion." *Nature Climate Change* 10, no. 3: 260–263. https://doi.org/10.1038/s41558-020-0697-0.

Wada, E., and A. Hattori. 1971. "Spectrophotometric Determination of Traces of Nitrite by Concentration of Azo Dye on an Anion-Exchange Resin: Application to Sea Waters." *Analytica Chimica Acta* 56, no. 2: 233–240. https://doi.org/10.1016/S0003-2670(01)82417-X.

Walters, W., E. R. Hyde, D. Berg-Lyons, et al. 2015. "Improved Bacterial 16S rRNA Gene (V4 and V4-5) and Fungal Internal Transcribed Spacer Marker Gene Primers for Microbial Community Surveys." *mSystems* 1, no. 1: e00009-15. https://doi.org/10.1128/msystems.00009-15.

Wickham, H. 2016. *ggplot2: Elegant Graphics for Data Analysis*. New York: Springer-Verlag. https://ggplot2.tidyverse.org.

Wilson, S. J., I. C. Anderson, B. Song, and C. R. Tobias. 2023. "Temporal and Spatial Variations in Subterranean Estuary Geochemical Gradients and Nutrient Cycling Rates: Impacts on Groundwater Nutrient Export to Estuaries." *Journal of Geophysical Research: Biogeosciences* 128, no. 6: e2022JG007132. https://doi.org/10.1029/2022JG007132.

Wood, E. D., F. a. J. Armstrong, and F. A. Richards. 1967. "Determination of Nitrate in Sea Water by Cadmium-Copper Reduction to Nitrite." *Journal of the Marine Biological Association of the United Kingdom* 47, no. 1: 23–31. https://doi.org/10.1017/S002531540003352X.

Wu, Y., Y. Wei, J. S. P. Ibánhez, et al. 2023. "Microbiota of a Seepage Face at the Mouth of a Subterranean Estuary: Diversity, Distribution and Substrate Dependence." *Acta Oceanologica Sinica* 42, no. 8: 147–157. https://doi.org/10.1007/s13131-023-2257-8.

Yamashita, Y., and E. Tanoue. 2003. "Chemical Characterization of Protein-Like Fluorophores in DOM in Relation to Aromatic Amino Acids." *Marine Chemistry* 82, no. 3: 255–271. https://doi.org/10.1016/S0304-4203(03)00073-2.

Ye, Q., J. Liu, J. Du, and J. Zhang. 2016. "Bacterial Diversity in Submarine Groundwater Along the Coasts of the Yellow Sea." *Frontiers in Microbiology* 6: 1519. https://doi.org/10.3389/fmicb.2015.01519.

Yilmaz, P., L. W. Parfrey, P. Yarza, et al. 2014. "The SILVA and "All-Species Living Tree Project (LTP)" Taxonomic Frameworks." *Nucleic Acids Research* 42, no. D1: D643–D648. https://doi.org/10.1093/nar/gkt1209.

Zsolnay, A., E. Baigar, M. Jimenez, B. Steinweg, and F. Saccomandi. 1999. "Differentiating With Fluorescence Spectroscopy the Sources of Dissolved Organic Matter in Soils Subjected to Drying." *Chemosphere* 38, no. 1: 45–50. https://doi.org/10.1016/S0045-6535(98)00166-0.

Appendix A

Detailed Fluorescent Dissolved Organic Matter Methods

Sample excitation (240–500 nm) and emission (250–825 nm) matrices were subtracted from deionized water blanks. Fluorescence values were scaled to Raman units by dividing sample values by the intensity of excitation at 350 nm in averaged deionised water blanks over an integrated emission range of 381–426 nm. Fluorescence intensities at specific excitations and emissions were taken from the literature. Coble A, B, C, M, and T are derived from Coble (1996) and Coble (2007). Coble A (450 nm emission intensity at 320 nm excitation) and Coble C (445 nm, 345 nm) are associated with terrestrial humic-like substances. Coble M (410 nm, 310 nm) is associated with autochthonous humic-like substances in marine and freshwater systems. M:C is the ratio of Coble M to Coble C, predominantly marine to terrestrial humics (Burdige, Kline, and Chen 2004). Coble T (340 nm, 275 nm) is associated with aromatic tryptophan-like substances. Coble B (305 nm, 275 nm) is associated with tyrosine-like substances. Fpeak (299 nm, 240 nm) is associated with phenylalanine (Yamashita and Tanoue 2003). Stedmon D (305 nm, 390 nm) is associated with terrestrial fulvic acid (Stedmon and Markager 2005). Emissions at 435 nm with 360 nm excitation are associated with optical brighteners (Hussain et al. 2012). Emissions at 360 nm with 240 nm excitation are associated with lignin (Hernes et al. 2009). FI (ratio of emission intensity at 450 nm to that at 500 nm obtained with an excitation of 370 nm) is an index to distinguish between microbially-derived fulvic acids (value of 1.9) and terrestrially-derived fulvic acids (value of 1.4) (McKnight et al. 2001). HIX (ratio of two spectral region areas from 300–345 nm to 435–480 nm at an excitation of 254 nm) is an index for the degree of humification and degradation of organic matter with higher values indicating more complex molecules like high molecular weight aromatics (Huguet et al. 2009; Zsolnay et al. 1999). BIX (ratio of emission intensity at 380 nm to that at 430 nm obtained with an excitation of 310 nm) is an index that signifies the presence of the b fluorophore indicating autochthonous biological activity (Huguet et al. 2009). BIX values over 1 correspond to the predominantly autochthonous origin of DOM.

Detailed Cell Count Methods

Samples fixed with paraformaldehyde were thawed at room temperature immediately prior to capturing the cells on a 0.1-μm Isopore membrane filter (Millipore, Cat. No. VCTP02500). Cells were prepared for microscopy by vacuum filtering 1 mL of sample was mixed with 1 mL of Milli-Q, then washed with 2 mL of PBS followed by 2 mL of a 1:1 PBS to ethanol solution. Finally, 2 mL of ethanol was added to the filter and incubated for 5 minutes before running through the filter. A quarter of the filter was mounted onto a slide and stained with 3 μL of DAPI, then kept in the dark for at least 15 min prior to imaging. DAPI-stained cells were imaged using a Nikon Eclipse Ti inverted epifluorescence microscope at 100× resolution. Cells were counted in at least three separate images using ImageJ (v1.53t). Prior to analyzing cell counts, each image had the background removed with a rolling ball radius of 50.0 pixels, the thresholds were set to remove grid lines and remaining noise for each image, cells were filled, and then the image was converted to a mask before separating clumped cells with the watershed function. Cells were counted using analyzer Particles with a size threshold of 10 square pixels. Cell counts were converted to cells per volume of sample, and mean cell counts from all analysed images were adopted as the cell density in each sample.

Detailed DNA Extraction Methods

Immediately prior to extraction, filters in their casing were thawed on ice, and then the casing was removed with PVC cutters sterilized with 70% ethanol. Half of the filter was cut into strips with a sterile scalpel and placed in a bead-beating tube. The remaining half of the filter was immediately returned to −80°C storage. 600 μL of Solution PM1 and 6 μL of DL-1, 4-Dithiothreitol (Fisher Scientific, Cat. No. AC426380100) were added and briefly vortexed. Bead beating occurred twice for 30 s at 5.5 m/s with 5 min of rest with a FastPrep-24 Classic (MP Biomedicals, Cat. No. 116004500). Chemical lysis was performed by adding 200 μg/mL of proteinase K (Millipore Sigma, Cat. No. 71-049-3) and incubating for 1 h at 55°C on a roller table. The remainder of the DNA extraction was performed to prepare samples for processing with a QIAcube Connect (QIAGEN, Cat. No. 9002864) using the manufacturer's protocol. Five sterile, unused filters were run in parallel during the sample DNA extractions as negative controls ('kitome'). To verify extractions were successful, DNA concentrations were immediately measured using 2 μL of the template with the Qubit dsDNA HS Assay (ThermoFisher, Cat. No. Q33230) according to manufacturer instructions. DNA extracts were stored at −80°C until shipping for amplicon sequencing (within 2 months).

Detailed 16S rRNA Gene Sequencing Methods

16S rRNA gene (V4) amplicon sequencing for samples and "kitome" controls was performed by the University of Michigan Microbiome Core. 96-well plates were loaded with DNA extracts where DNA concentrations were diluted to less than 5 ng/μL when necessary with nuclease-free sterile water (QIAGEN, Cat. No. 129112). Plates were sealed and frozen overnight at −80°C before being shipped on dry ice to the sequencing core. At the core facility, samples were stored at −80°C (approximately 2 months) until PCR amplicons were generated for the V4 region of the 16S rRNA gene using the modified 515 forward (5′-GTGYCAGCMGCCGCGGTAA-3′) and 806 reverse (5′-GGACTACNVGGGTWTCTAAT-3′) Earth Microbiome Project primers (Walters et al. 2015). DNA amplicons were sequenced across two separate runs on a 2 × 250 Illumina MiSeq v2. Per plate, a nuclease-free sterile water PCR negative control and a mock community positive control (ZymoBIOMICS, Cat. No. D6306) were included by the Microbiome Core in addition to field blanks and extraction blanks ('kitome').

Sequences were provided in demultiplexed fastq files. The forward and reverse reads were trimmed at 240 base pairs (bp) and 200 bp, respectively. Reads underwent quality control where reads were removed if ambiguous bases were present, contained more than two expected errors, or originated from PhiX, and reads were truncated after the first occurrence of a base with a Q-score less than two. Using the DADA2 pipeline (v1.22.0, Callahan et al. 2016), reads were then dereplicated, denoised, and merged. Singletons, chimeric sequences, and reads with lengths less than 250 bp or greater than 260 bp were removed. Resulting amplicon sequence variants (ASVs) were assigned taxonomic information with the SILVA nr99 database (v138.1, Quast et al. 2013; Yilmaz et al. 2014). Decontamination of ASVs with greater frequency and prevalence in the kitome and PCR negative controls was performed with Decontam (v1.14.0, Davis et al. 2018) using the 'either' method and a threshold of 0.1. Decontamination removed 857 ASVs while retaining 65,719 ASVs. ASVs identified as chloroplasts or mitochondria were also removed from the dataset (1,425 ASVs), retaining 63,344 total unique ASVs for analysis. There were 7,613,584 total reads in the resulting dataset. The median sequencing depth per sample was 33,353 reads (range = 7816–92,556 reads).

TABLE A1 | The effect of spatial and temporal variation on physicochemical measurements. Kruskal-Wallis rank sum test chi-squared statistic for environmental data.

Variable	*n*	Well	Depth	Well*Depth	Well*Season	Season	Date	Tide regime (S/N)	Tide (HH/LL)	Season*Tide
Salinity (PSU)	516	233.9***	114.5***	404.1***	278.7***	10.8	40.8	4.2	0.1	11.0
Temperature (°C)	516	36.1***	106.3***	341.6***	410.***	384.0***	412.5***	143.7***	3.8	386.2***
DO (μM)	516	39.5***	79.7 ***	277.4 ***	55.9 ***	6.9	24.0	7.2	3.5	14.6
pH	515	22.9**	262.0 ***	381.4***	173.7***	27.0***	44.3*	20.6**	2.0	27.4**
Ammonia (μM)	514	123.6***	168.6***	378.0***	172.4***	48.2***	56.4***	10.2	0.0	44.4***
Nitrate (μM)	515	14.0	274.7***	418.9***	86.6***	38.8***	78.6***	16.9**	0.2	36.0***
Nitrite (μM)	515	102.2***	80.6***	416.9***	207.2***	92.5***	107.3***	24.7***	0.2	82.8***
Phosphate (μM)	515	247.8***	108.1***	375.9***	274.0***	1.1	43.2	6.3	0.2	3.2
Cell count (mL^{-1})	171	63.3***	53.8***	92.4***	74.5***	6.4	13.2	3.6	1.2	n.m.
DOC (μM)	180	103***	46.8***	123.8***	108.6***	0.0	15.2	1.3	0.0	n.m.
Coble A (RFU)	180	105.5***	47.9***	138.8***	112.4***	0.9	10.6	1.5	0.0	n.m.
Coble B (RFU)	180	94.2***	42.5***	134.9***	106.8***	10.0	20.0	5.8	0.1	n.m.
Coble C (RFU)	180	102.1***	47.3***	136.9***	109.5***	1.5	11.1	1.9	0.0	n.m.
Coble M (RFU)	180	106.8***	48.2***	140.0***	113.8***	0.6	10.1	1.1	0.0	n.m.
Coble T (RFU)	180	94.9***	41.7***	133.5***	105.5***	6.4	16.6	3.4	0.2	n.m.
Fpeak (RFU)	180	73.0***	35.5*	99.6***	87.2***	8.3	18.8	3.5	0.0	n.m.
Stedmon D (RFU)	180	97.6***	47.3***	131.7***	107.1***	3.4	15.1	4.5	0.0	n.m.
OB (RFU)	180	99.1***	46.6***	134.1***	107.4***	1.7	11.9	2.1	0.0	n.m.
Lignin (RFU)	180	87.8***	38.1**	137.7***	103.1***	8.9	18.1	2.7	0.0	n.m.
HIX	180	57.7***	26.7	109.6***	66.0***	0.1	6.2	1.2	0.5	n.m.
BIX	180	96.9***	46.9***	135.1***	106.2***	1.7	11.0	0.7	0.0	n.m.
FI	180	49.0***	43.3***	119.5***	110.9***	32.3***	42.8***	6.4	0.2	n.m.
M:C	180	111.4***	51.5***	139.9***	119.0***	0.0	8.3	0.2	0.0	n.m.

Note: N, number of observations; S/N, spring/neap tide; DO, dissolved oxygen; DOC, dissolved organic carbon; n.m., not measured; OB, optical brightener. Significance codes: 0 '***' 0.001 '**' 0.01 '*' 0.05 *p* values from Bonferroni correction.

TABLE A2 | Median (min-max) for physicochemical and nutrient measurements are separated by region within the subterranean estuary and season.

	Shallow		Intermediate		Deep		Well 4		Seawater	
	Feb-22	**Oct-22**	**Feb-22**	**Oct-22**	**Feb-22**	**Oct-22**	**Feb-22**	**Oct-22**	**Feb-22**	**Oct-22**
n	105	34	36	34	34	153	69	51	16	9
Salinity (PSU)	3.2 (0.7–32.8)	1.9 (0.7–3.9)	5.1 (0.8–18.7)	1.0 (0.9–1.6)	6.8 (3.6–10.7)	6.0 (2.9–16.4)	29.1 (11.8–34.5)	10.0 (7.9–12.1)	32.5 (31.8–33.4)	33.1 (32.7–33.5)
Temperature (°C)	13.8 (8.5–15.7)	17.9 (14.8–19.5)	13.6 (10.3–15.1)	17.9 (15.2–19.6)	13.9 (10.2–15.8)	17.5 (15.1–20.1)	11.9 (8.8–13.6)	17.6 (16.1–19.3)	12.2 (9.6–14.0)	15.5 (14.3–17.4)
DO (μM)	206.3 (40.3–357.2)	144.5 (100.3–321.3)	79.5 (38.8–175.6)	128.0 (94.7–308.8)	145.3 (47.8–305.6)	139.7 (16.3–317.2)	253.4 (90.6–320.3)	164.4 (99.1–316.3)	278.1 (267.2–322.8)	284.7 (265.3–295.0)
pH	8.5 (7.9–9.3)	8.8 (8.5–8.9)	8.5 (7.9–9.1)	8.0 (7.6–8.4)	7.9 (7.4–8.3)	7.9 (7.5–8.3)	7.9 (7.5–8.2)	8.1 (8.0–8.4)	8.0 (7.5–8.2)	8.0 (8.0–8.1)
Nitrate (μM)	252.9 (54.4–553.5)	391.4 (189.9–511.4)	220.6 (66.8–482.9)	238.0 (168.8–313.7)	27.4 (0.0–188.3)	9.8 (0.0–256.3)	90.6 (11.7–224.7)	90.7 (47.5–129.4)	14.9 (9.1–32.0)	9.1 (5.7–9.9)
Nitrite (μM)	1.0 (0.0–112.2)	8.7 (4.3–19.8)	0.3 (0.0–4.1)	16.3 (12.7–22.9)	0.8 (0.0–4.1)	2.1 (0.0–23.8)	0.0 (0.0–0.9)	3.0 (0.0–7.1)	0.2 (0.0–0.4)	0.6 (0.0–0.9)
Ammonia (μM)	1.6 (0.0–34.4)	1.5 (0.7–3.3)	0.2 (0.0–1.5)	1.2 (0.0–4.2)	3.0 (0.6–41.0)	6.7 (0.0–53.0)	0.1 (0.0–7.9)	1.2 (0.0–13.9)	0.7 (0.0–2.2)	3.3 (1.2–5.7)
Phosphate (μM)	24.5 (4.4–73.3)	22.9 (12.1–84.7)	15.9 (9.5–71.4)	11.9 (0.0–85.1)	47.7 (20.3–90.6)	29.4 (0.0–74.1)	3.8 (1.2–6.6)	6.4 (0.0–30.9)	2.1 (1.5–6.8)	1.8 (0.0–56.1)

Abbreviations: DO, dissolved oxygen; *n*, number of observations (third row).

TABLE A3 | Median (min-max) values for cell abundance and organic matter measurements separated by region within the subterranean estuary and season.

	Shallow		Intermediate		Deep		Well 4		Seawater	
	Feb-22	**Oct-22**	**Feb-22**	**Oct-22**	**Feb-22**	**Oct-22**	**Feb-22**	**Oct-22**	**Feb-22**	**Oct-22**
n	57	6	20	6	19	27	36	9	5	3
Cells ml^{-1} (x 10^5)	5.6 (1.4–48.7)	5.6 (1.1–6.2)	3.6 (2.3–8.1)	7.6 (5.5–8.8)	4.1 (1.9–11.6)	5.7 (2.3–11.6)	1.7 (0.6–5.9)	3.7 (1.9–6.9)	8.3 (6.6–10.1)	27.1 (25.2–29.0)
DOC (μM)	636.8 (192.2–962.6)	517.4 (440.6–544.3)	486.4 (178.5–807.3)	543.3 (524.2–590.6)	453.0 (210.7–807.3)	481.5 (301.6–769.9)	117.8 (74.2–307.5)	290.1 (263.3–305.6)	79.3 (76.7–90.0)	96.4 (96.0–98.1)
TDN (μM)	331.3 (56.0–589.6)	413.1 (330.9–469.1)	312.2 (62.2–469.9)	287.5 (240.5–320.9)	75.1 (30.7–384.9)	75.4 (48.8–265.3)	119.5 (25.8–246.6)	120.2 (101.9–145.5)	20.2 (16.3–23.3)	24.1 (23.4–24.8)
Coble A (RFU)	0.57 (0.51–0.63)	0.55 (0.55–0.56)	0.53 (0.50–0.65)	0.54 (0.53–0.55)	0.55 (0.51–0.69)	0.55 (0.50–0.61)	0.23 (0.04–0.51)	0.51 (0.51–0.52)	0.04 (0.04–0.07)	0.05 (0.05–0.05)
Coble B (RFU)	0.07 (0.04–0.22)	0.07 (0.06–0.09)	0.05 (0.02–0.09)	0.07 (0.06–0.07)	0.07 (0.05–0.19)	0.08 (0.04–0.14)	0.02 (0.00–0.04)	0.05 (0.04–0.06)	0.02 (0.01–0.02)	0.03 (0.01–0.03)
Coble C (RFU)	0.46 (0.42–0.50)	0.46 (0.45–0.46)	0.44 (0.42–0.52)	0.45 (0.44–0.45)	0.45 (0.42–0.55)	0.46 (0.42–0.49)	0.22 (0.03–0.43)	0.43 (0.43–0.44)	0.04 (0.04–0.06)	0.05 (0.04–0.05)
Coble M (RFU)	0.73 (0.63–0.82)	0.70 (0.69–0.72)	0.67 (0.63–0.69)	0.68 (0.67–0.69)	0.69 (0.65–0.91)	0.70 (0.63–0.79)	0.24 (0.04–0.64)	0.64 (0.64–0.66)	0.05 (0.05–0.07)	0.06 (0.06–0.07)
Coble T (RFU)	0.31 (0.14–0.64)	0.31 (0.24–0.34)	0.23 (0.14–0.41)	0.29 (0.28–0.63)	0.30 (0.23–0.63)	0.33 (0.17–0.54)	0.06 (0.01–0.22)	0.22 (0.20–0.26)	0.02 (0.02–0.03)	0.05 (0.03–0.07)
Fpeak (RFU)	0.06 (0.01–0.16)	0.07 (0.03–0.10)	0.03 (0.02–0.07)	0.05 (0.04–0.07)	0.05 (0.03–0.10)	0.07 (0.00–0.15)	0.01 (0.00–0.05)	0.04 (0.01–0.06)	0.00 (0.00–0.02)	0.02 (0.00–0.03)
SD (RFU)	0.47 (0.36–0.49)	0.47 (0.46–0.47)	0.46 (0.39–0.50)	0.46 (0.45–0.46)	0.47 (0.44–0.53)	0.47 (0.44–0.48)	0.10 (0.02–0.36)	0.45 (0.41–0.46)	0.02 (0.02–0.03)	0.02 (0.02–0.03)
OB (RFU)	0.47 (0.43–0.51)	0.46 (0.46–0.47)	0.45 (0.43–0.52)	0.45 (0.45–0.46)	0.46 (0.43–0.55)	0.46 (0.43–0.55)	0.18 (0.03–0.44)	0.44 (0.44–0.45)	0.03 (0.03–0.05)	0.04 (0.03–0.04)
Lignin (RFU)	1.12 (0.53–1.78)	1.18 (0.94–1.35)	0.90 (0.56–1.53)	0.99 (0.94–1.03)	1.07 (0.87–2.33)	1.18 (0.58–1.90)	0.22 (0.03–0.63)	0.90 (0.84–1.01)	0.05 (0.04–0.08)	0.07 (0.06–0.09)
BIX	1.36 (0.87–1.38)	1.35 (1.34–1.36)	1.33 (0.92–1.39)	1.35 (1.34–1.35)	1.35 (1.33–1.40)	1.35 (1.03–1.38)	0.73 (0.64–0.87)	1.24 (1.15–1.34)	0.78 (0.76–0.83)	0.87 (0.84–0.92)
HIX	16.56 (5.93–20.97)	17.02 (16.11–17.56)	17.81 (15.67–19.58)	17.13 (16.25–17.70)	17.25 (12.20–19.60)	16.35 (10.92–17.94)	12.13 (4.13–17.24)	14.70 (14.14–15.49)	4.46 (3.93–5.36)	2.89 (2.52–3.54)
FI	1.03 (1.03–1.04)	1.03 (1.03–1.03)	1.03 (1.03–1.06)	1.03 (1.03–1.03)	1.03 (1.03–1.04)	1.03 (1.03–1.03)	1.40 (1.06–1.49)	1.03 (1.03–1.03)	1.54 (1.48–1.56)	1.51 (1.50–1.58)
M:C	0.63 (0.61–0.67)	0.65 (0.64–0.65)	0.66 (0.60–0.67)	0.66 (0.65–0.66)	0.65 (0.61–0.66)	0.65 (0.62–0.67)	0.89 (0.67–0.95)	0.67 (0.67–0.68)	0.80 (0.79–0.83)	0.79 (0.62–0.82)

Note: DOC, dissolved organic carbon; *n*, number of observations (third row); OB, optical brighteners; RFU, relative fluorescence units; SD, Stedmon D; TDN = total dissolved nitrogen. More information on the fDOM metrics can be found in the Appendix A (see "Appendix fluorescent dissolved organic matter methods").

TABLE A4 | The correlation (Mantel tests) of physicochemical variables with microbial community composition (Bray–Curtis dissimilarity matrix generated using ASV-level data) using combinations of season and region-based subsets of the porewater samples.

Dataset	*n*	Best set of variables (BIOENV)	Spearman's correlation (ρ)	Best singular variable	Spearman's correlation (ρ)	Best two variables	Spearman's correlation (ρ)
February	130	Salinity, DO, pH, nitrate, ammonia, phosphate, DOC, HIX, Fpeak	0.741	Phosphate	0.543	Nitrate, phosphate	0.628
October	48	Salinity, nitrate, phosphate, DOC	0.629	DOC	0.448	Nitrate, DOC	0.591
Intermediate, February	29	Salinity	0.690	Salinity	0.690	Salinity, nitrate	0.634
Intermediate, October	15	pH, nitrate, phosphate	0.832	Phosphate	0.641	Nitrate, phosphate	0.797
Deep, February	19	Salinity, nitrate, ammonia, HIX	0.855	Salinity	0.806	Salinity, HIX	0.808
Deep, October	24	Salinity, pH, nitrate, nitrite, ammonia	0.672	Salinity	0.515	Salinity, nitrate	0.638
Well 4, February	36	Nitrate, ammonium, HIX	0.548	HIX	0.470	Nitrate, HIX	0.537
Well 4, October	9	Salinity, HIX	0.700	Salinity	0.541	Salinity, HIX	0.541

TABLE A5 | Phyla, over 0.1% of the total sequencing reads, paired with the region where they were significantly enriched based on DESeq analysis. Log 2 fold change in the region compared to all other regions, standard error (linear discriminant analysis effect size, lfcSE), the Wald statistic, and Benjamini-Hochberg adjusted *p* values are reported.

Phylum	Region	log 2 fold change	lfcSE	Wald statistic	Adjusted *p*
Firmicutes	Shallow	3.26	0.38	8.58	9.88E-17
Bdellovibrionota	Shallow	2.45	0.21	11.77	1.70E-30
Bacteroidota	Shallow	1.72	0.21	8.38	4.10E-16
Proteobacteria	Shallow	1.26	0.16	7.83	2.20E-14
Thermoplasmatota	Shallow	1.21	0.40	3.07	4.94E-03
Methylomirabilota	Intermediate	2.63	0.54	4.90	8.28E-06
Elusimicrobiota	Intermediate	1.46	0.27	5.42	1.03E-06
Nitrospirota	Intermediate	1.32	0.32	4.10	1.42E-04
Acidobacteriota	Intermediate	1.09	0.20	5.44	1.03E-06
Myxococcota	Intermediate	0.88	0.20	4.47	3.44E-05
Planctomycetota	Intermediate	0.67	0.15	4.47	3.44E-05
Patescibacteria	Intermediate	0.54	0.13	4.30	6.61E-05
Verrucomicrobiota	Intermediate	0.42	0.16	2.67	1.91E-02
Campylobacterota	Deep	4.54	0.70	6.51	3.17E-10
Desulfobacterota	Deep	3.91	0.24	16.18	1.68E-57
Chloroflexi	Deep	2.40	0.18	13.31	2.70E-39
Aenigmarchaeota	Deep	1.72	0.35	4.93	2.56E-06
Nitrospirota	Deep	1.14	0.33	3.45	1.27E-03
Verrucomicrobiota	Deep	0.87	0.15	6.00	6.91E-09
Acidobacteriota	Deep	0.75	0.21	3.57	9.08E-04
Desulfobacterota	Deep	0.51	0.19	2.75	1.06E-02
Planctomycetota	Deep	0.46	0.16	2.98	5.63E-03
Nanoarchaeota	Well 4	1.40	0.18	7.82	1.60E-13
Desulfobacterota	Well 4	0.98	0.18	5.53	3.25E-07
Myxococcota	Well 4	0.72	0.21	3.41	2.01E-03
Actinobacteriota	Seawater	3.22	0.35	9.15	2.51E-18
Bacteroidota	Seawater	1.84	0.62	2.95	1.54E-02

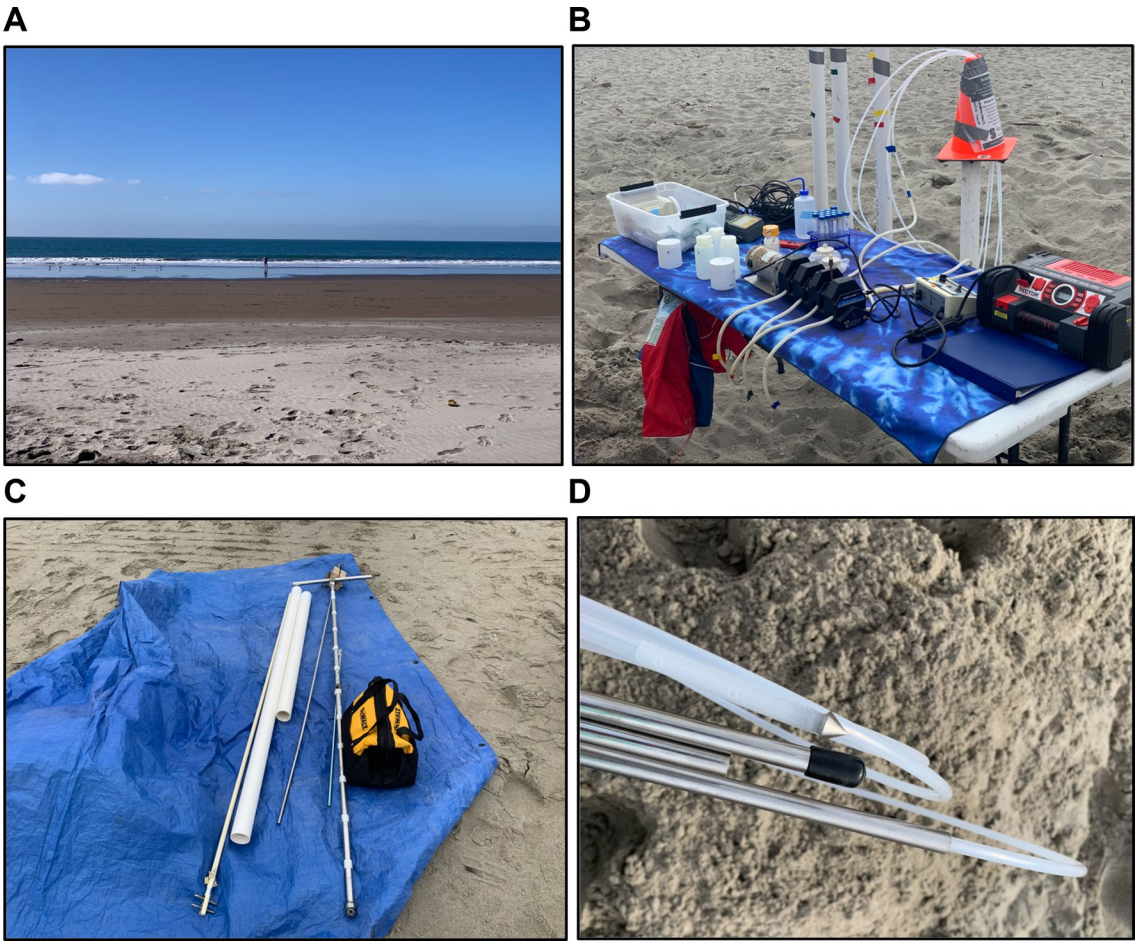

FIGURE A1 | Images from porewater sample collection at Stinson Beach, CA STE. (A) View to surf from Well 4 during L in February. (B) Peristaltic pump to collect porewater using SedPoint2 (M.H.E. Products) polyethylene tubing installed subsurface at each well location. (C) Installation tools (SedPoint Installer and hand-operated sand auger) and slotted PVC pipe before installation. (D) SedPoint2 halfway inserted into SedPoint Installer showing the two-inch screen and stainless steel tip.

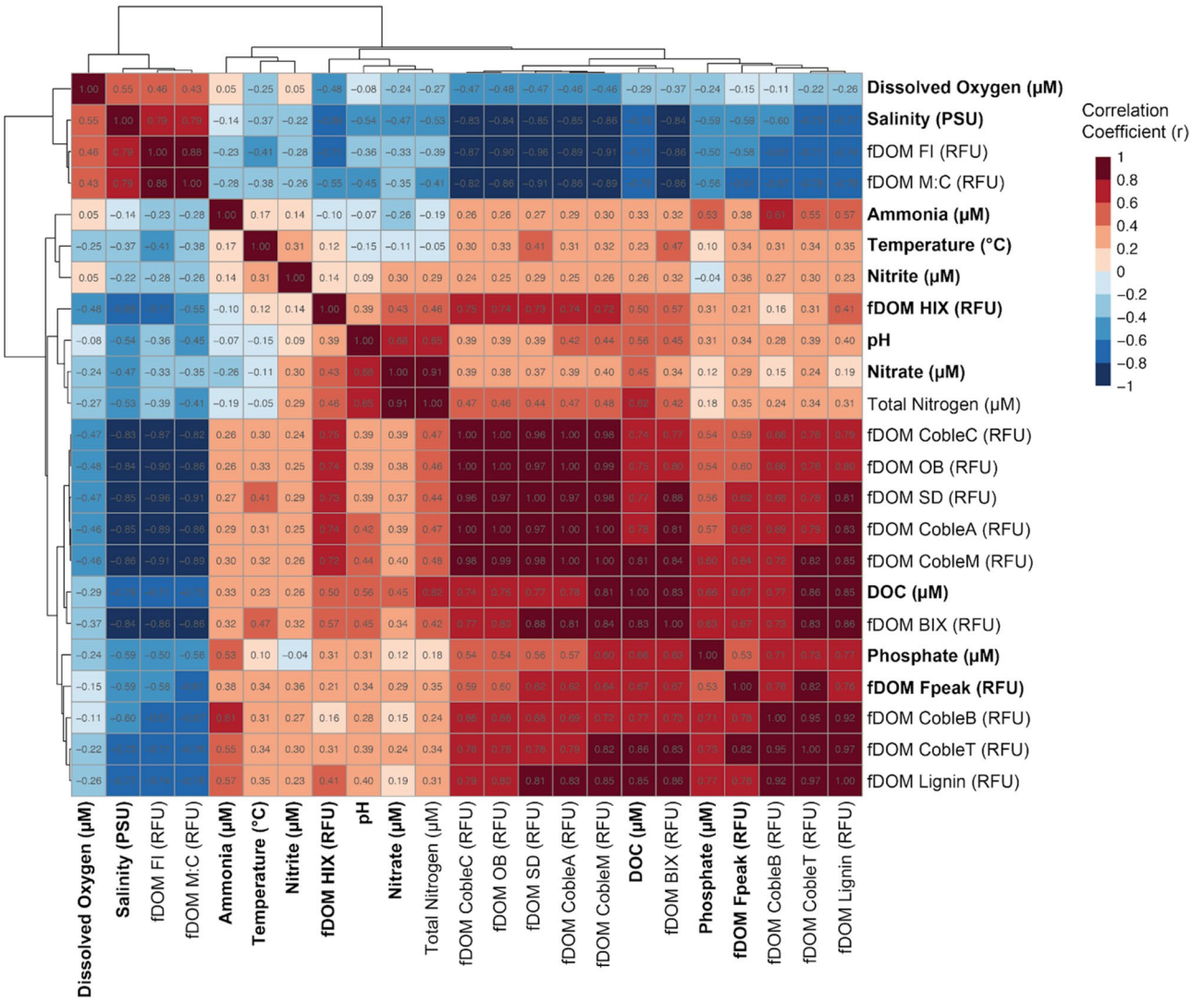

FIGURE A2 | Pairwise correlation matrix between environmental variables to assess multicollinearity. If two variables were highly correlated (Pearson's correlation coefficient > 0.8), one variable was chosen as a representative for downstream statistical analyses. The variables selected are shown in bold. Correlation computed with the cor function in the *stats* package and visualised with the pheatmap function and package. DOC = dissolved organic carbon. fDOM = fluorescent dissolved organic matter. Total nitrogen = inorganic and organic measured together by TOC-L.

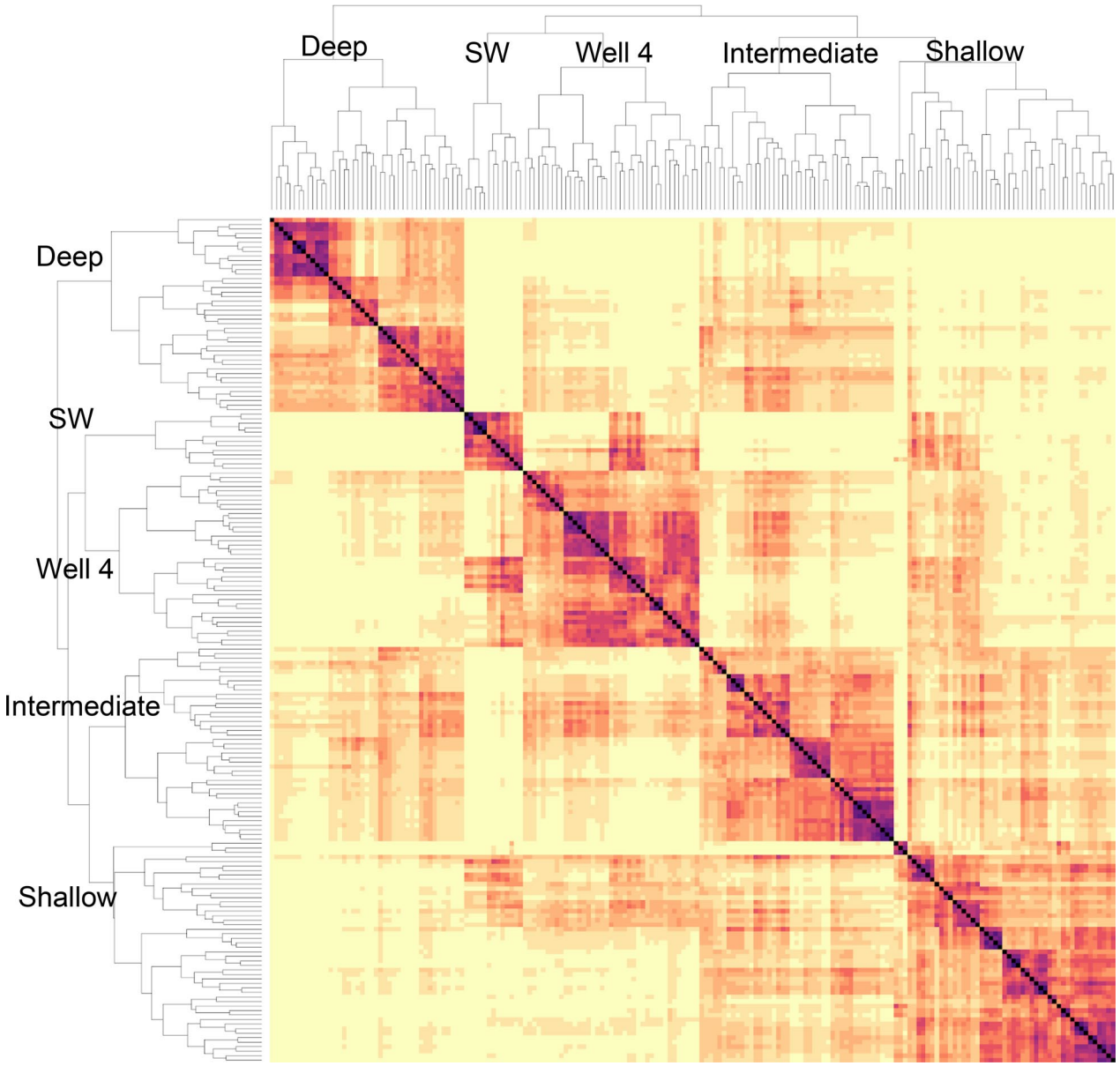

FIGURE A3 | Hierarchical clustering of samples based on Bray–Curtis dissimilarity of ASV data for each sample (each row and column). Clustering is computed with the hclust function and visualised with the heatmap function both in the stats package. SW = seawater samples.

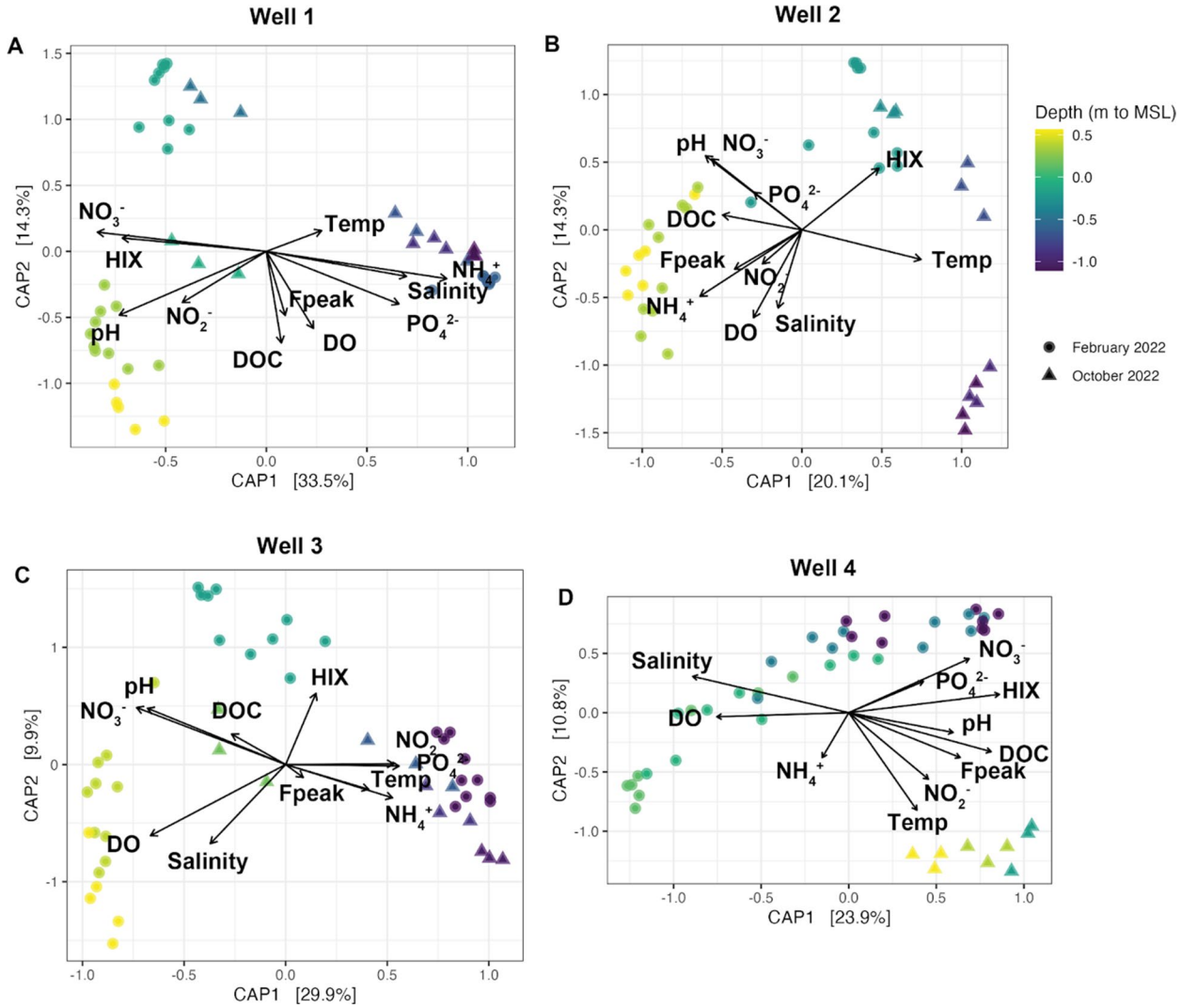

FIGURE A4 | Constrained analysis of principal coordinates (CAP) using the Bray–Curtis dissimilarity matrix and the reduced subset of environmental variables for each well analyzed separately (A–D). Samples are plotted as circles (February 2022) or triangles (October 2022). The color of each sample represents the depth in meters to mean sea level (MSL).

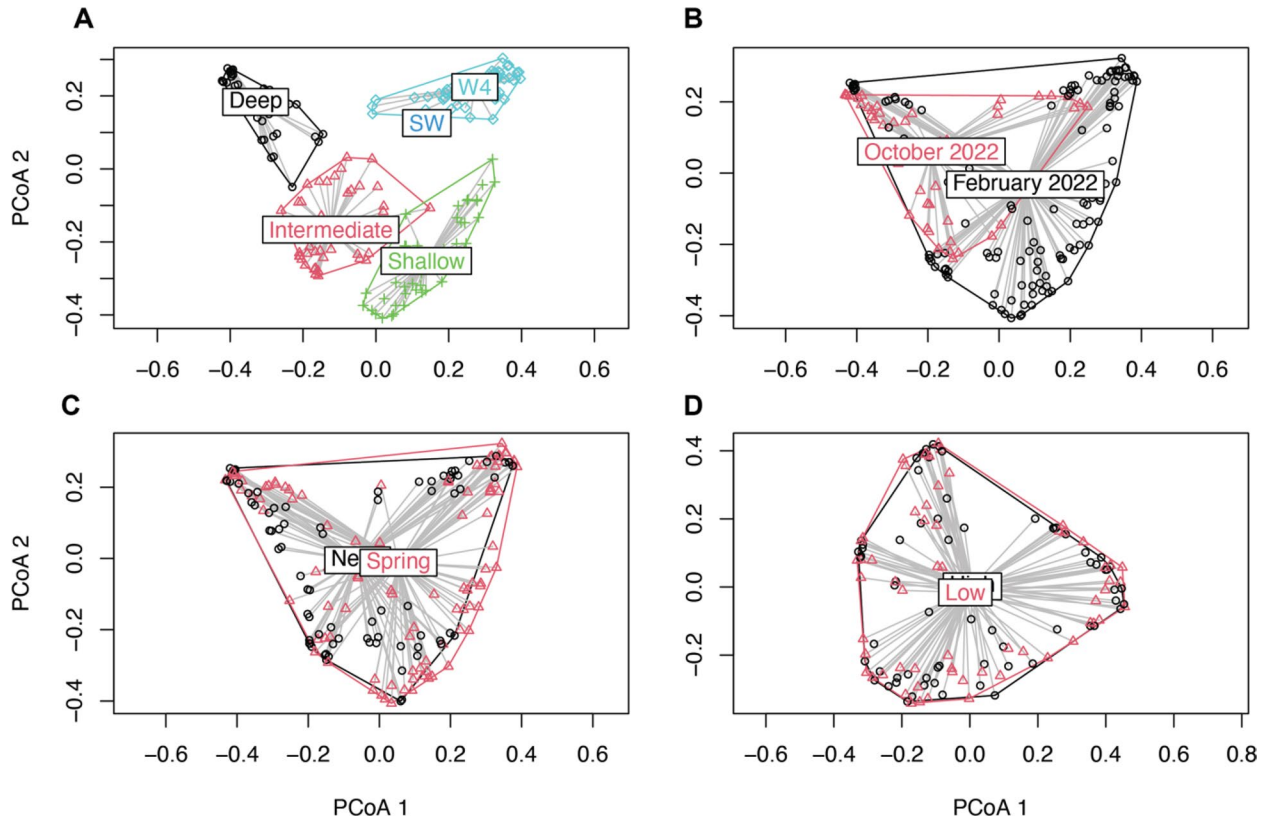

FIGURE A5 | Convex hull depictions using principal coordinates of microbial community variation (Bray–Curtis dissimilarity matrix generated using ASV-level data for each sample) showing groupings of region (A), season (B), tidal regime (spring/neap) (C), and tide (H/L) (D). Labels are positioned at the centroid, where increasing overlap decreases dissimilarity between groups. Seawater (SW) samples are shown in A for comparison but not included in the temporal comparisons (B, C, or D) or statistical tests in Table 2. The tide (H/L) comparison (D) was only possible during the February sampling.

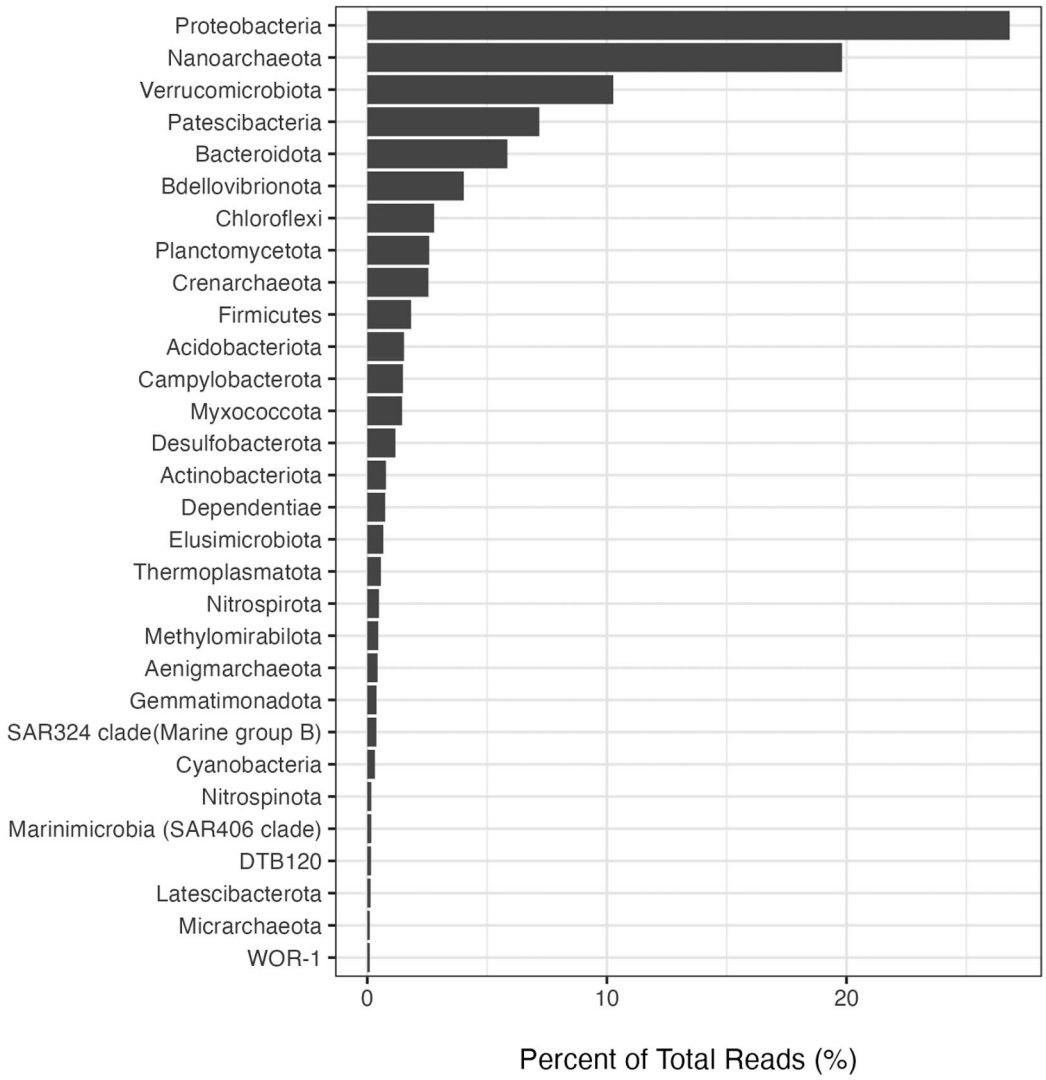

FIGURE A6 | Rank-abundance curve of the phyla with abundance over 0.1% of the total sequencing reads for all samples ($n = 187$) and ordered by contribution to total reads. These phyla represent 95.4% of total reads collectively and 30/80 of the total classified phyla.

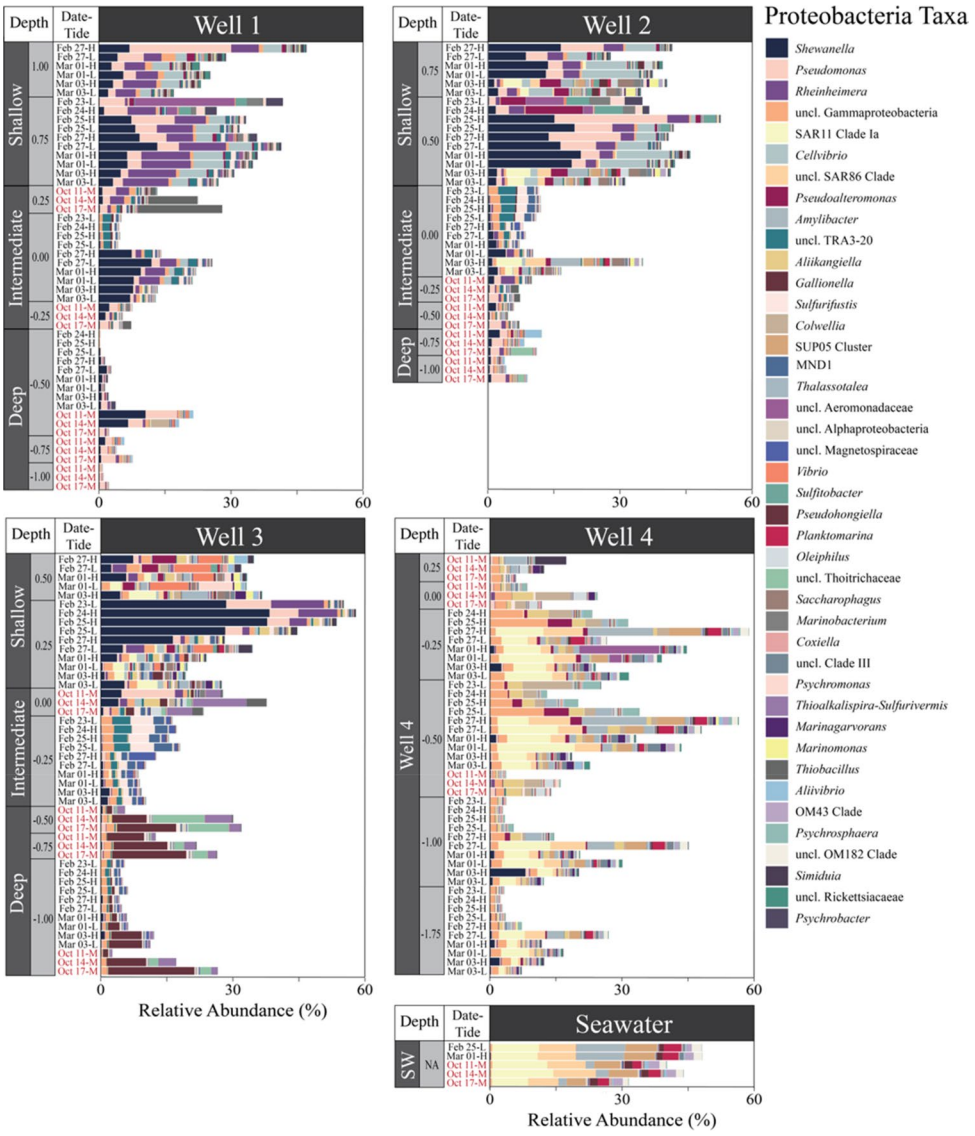

FIGURE A7 | Relative abundance of Proteobacteria taxa out of the total sequencing reads for each porewater ($n = 182$) and seawater (SW) sample ($n = 5$). Taxa displayed are over 0.5% of the Proteobacteria reads and ordered by overall abundance. These taxa represent 19.8% of total reads. Samples are separated by well and then ordered by depth, date, and tide, where depth is a 0.25 m depth bin relative to mean sea level (MSL). Samples collected in October are highlighted in red text. Well 4 is closest to the surf zone where seawater samples were collected. Clustered regions are noted vertically along the side of each panel. uncl. = unclassified at the genus level with the finest taxonomic resolution following.

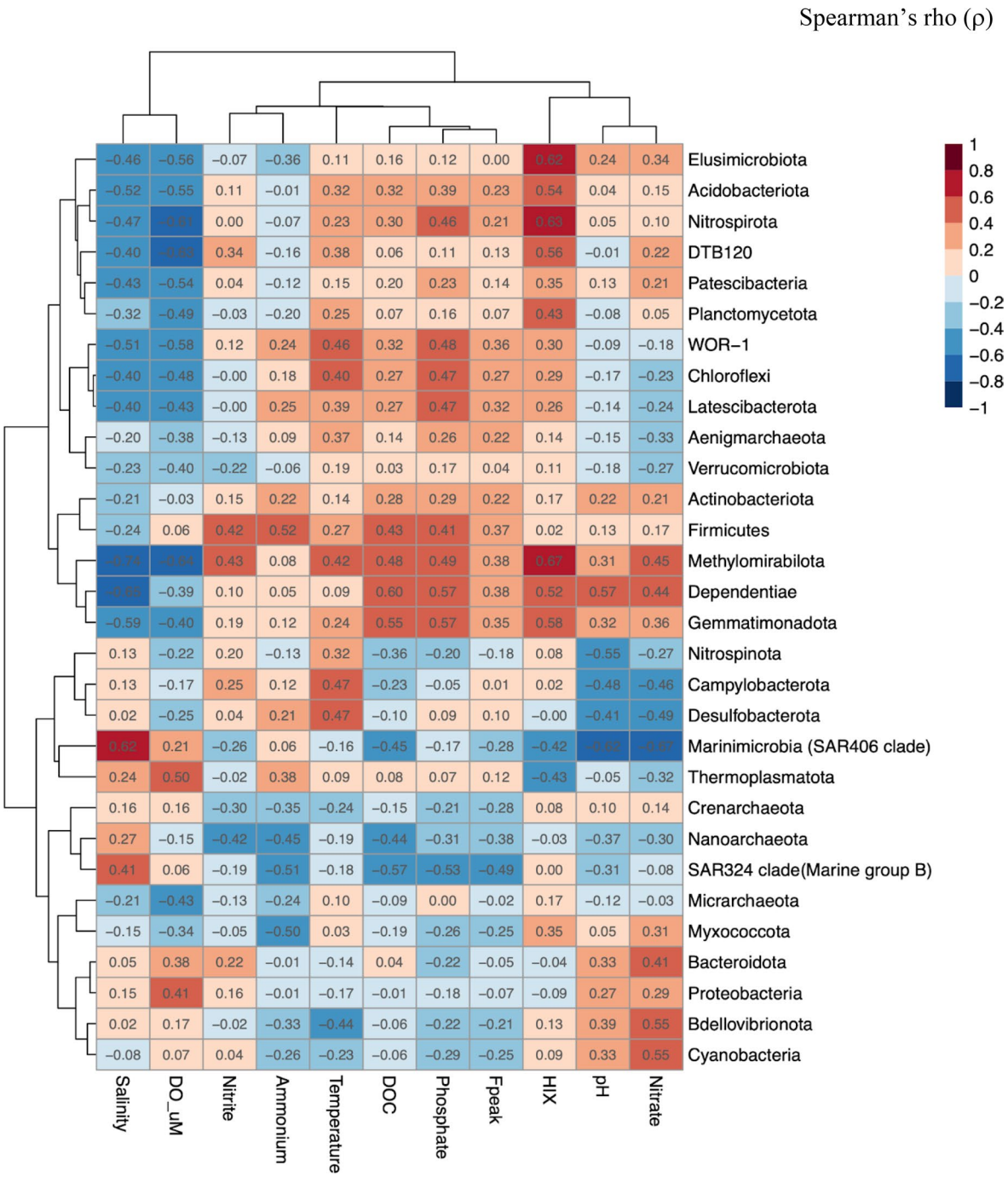

FIGURE A8 | Pairwise Spearman's rank correlation matrix of the phyla with abundances over 0.1% of the total sequencing reads with the reduced subset of environmental variables. Clustering for the dendrogram is hierarchical based on the matrix results. DO = dissolved oxygen. DOC = dissolved organic carbon. HIX = humification index.

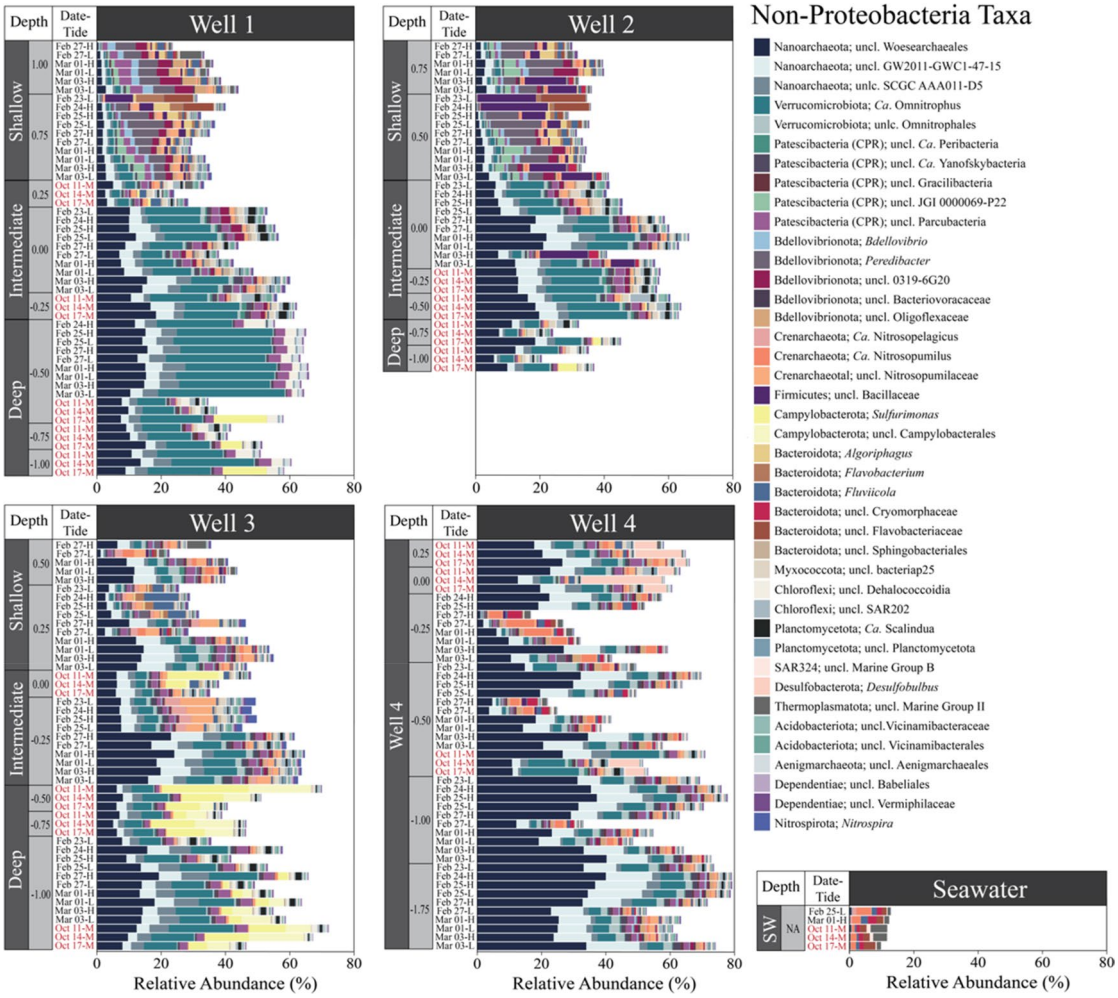

FIGURE A9 | Relative abundance of non-Proteobacteria taxa out of total sequencing reads for each porewater ($n = 182$) and seawater (SW) sample ($n = 5$). Taxa displayed are individually over 0.25% of total reads and collectively represent 50.8% of total reads. Samples are separated by well and then ordered by depth, date, and tide, where depth is a 0.25 m depth bin relative to mean sea level (MSL). Samples collected in October are highlighted in red text. Well 4 is closest to the surf zone where seawater samples were collected. Clustered regions are noted vertically along the side of each panel. uncl. = unclassified at the genus level with the finest taxonomic resolution following.

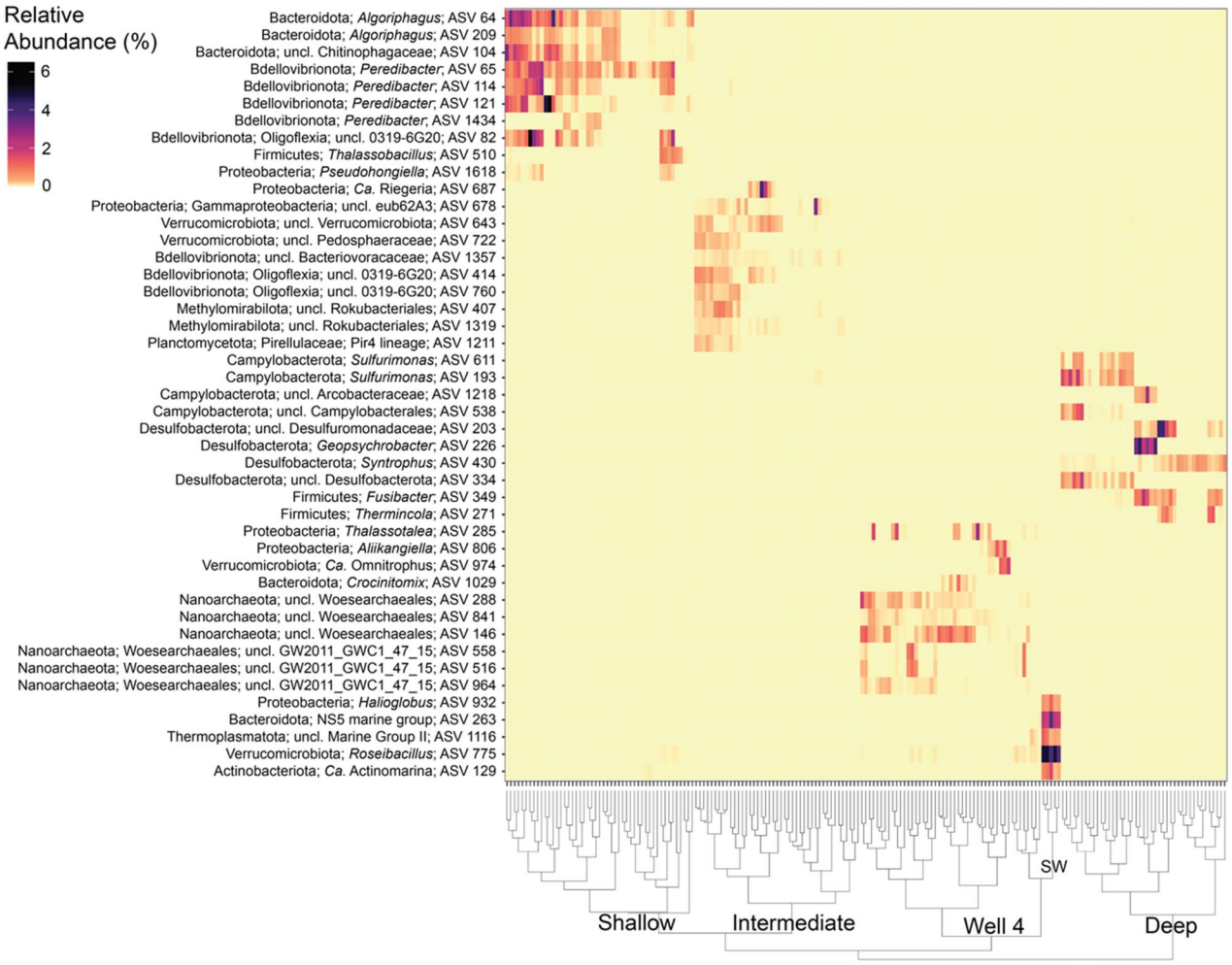

FIGURE A10 | Heatmap of the relative abundance (per cent of total reads per sample) of the STE region indicator ASVs across all porewater and seawater surf samples. Samples were clustered based on the Bray–Curtis dissimilarity matrix of all 63,344 ASVs. The hierarchical cluster dendrogram is displayed with the region labels. Seawater (SW) samples cluster with a branch of the Well 4 samples that were impacted by the overtopping event in February 2022. uncl. = unclassified at the genus level with the finest taxonomic resolution following.

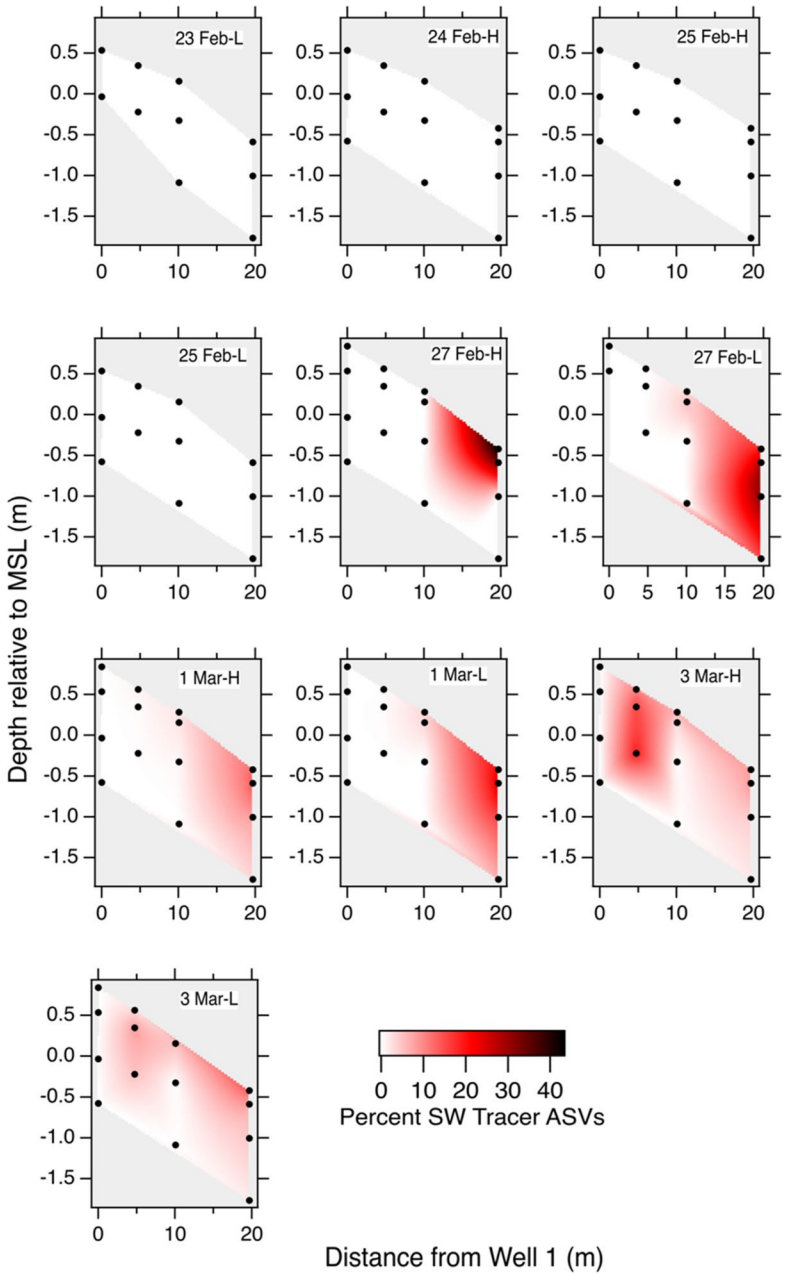

FIGURE A11 | Cross-sectional maps of percent seawater tracer ASVs (sum of the reads assigned as seawater tracer ASVs divided by the total reads for each sample) through time. ASVs are defined in the text. Panels show progressive time points during sampling from the L tide on 23 February to the L tide on 3 March 2022. Overtopping water due to waves occurred at Well 4 during H tide on 27 February.

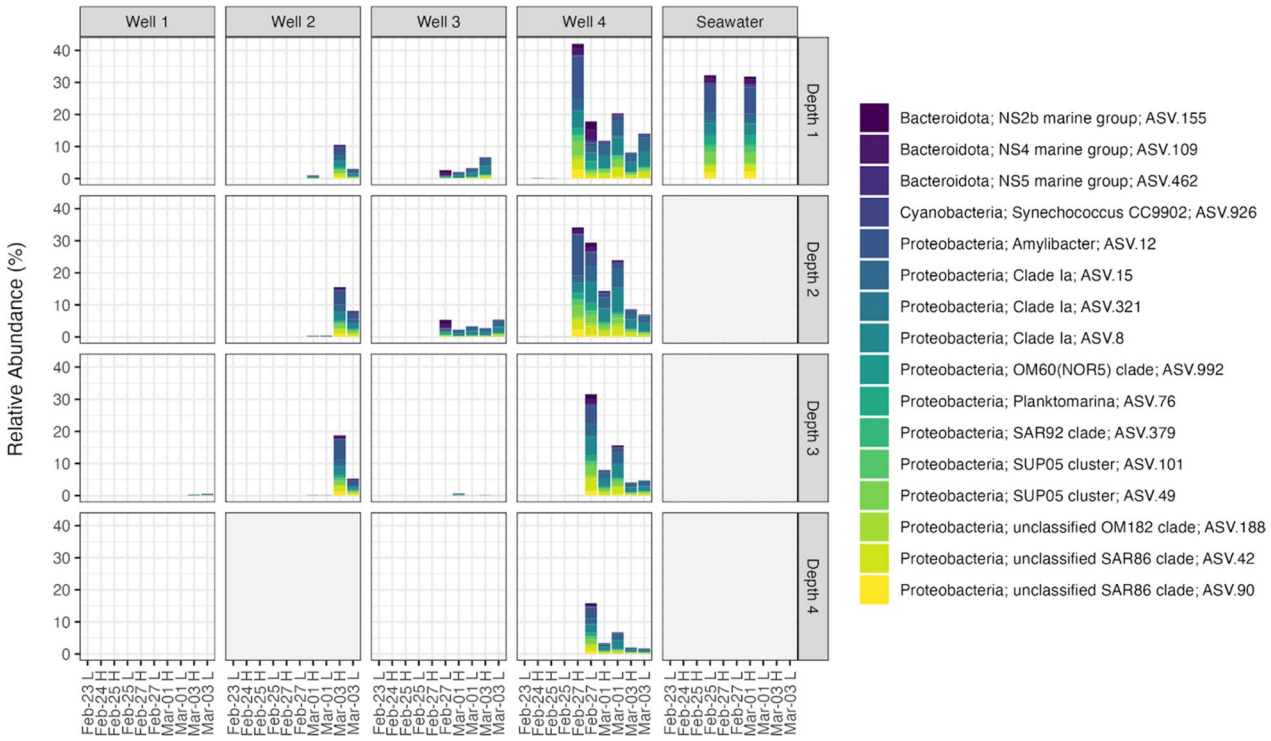

FIGURE A12 | Seawater tracer ASVs depicting the spread and rate of influence of the wave set in February 2022. Relative abundance out of the total sequencing reads per sample. These 16 ASVs were identified with DESeq2 as significantly enriched in seawater versus porewater prior to February 27. Samples are organised by Well (columns) and Depth (rows), where depth is relative within each well. The *x*-axis is the date and tide (H/L) in order of sampling. No samples were collected at greyed out locations.